Spring 2018

Biogeochemical Cycling of Selenium in the Arctic Ocean

Kyle M. McQuiggan
Old Dominion University, mcquiggk@gmail.com

BIOGEOCHEMICAL CYCLING OF SELENIUM IN THE AMERASIAN BASIN

by

Kyle A. McQuiggan
B.S. June 2014, Union College

A Thesis Submitted to the Faculty of Old Dominion University in Partial Fulfillment of the Requirements for the Degree of

MASTER OF SCIENCE

OCEAN, AND EARTH SCIENCES

May 2018

Approved by:

Gregory A. Cutter (Director)

Dennis A. Darby (Member)

H. Rodger Harvey (Member)

ABSTRACT

BIOGEOCHEMICAL CYCLING OF SELENIUM IN THE AMERASIAN BASIN

Kyle A. McQuiggan
Old Dominion University, 2018
Director: Dr. Gregory A. Cutter

Changes in the global climate may have a pronounced effect on the biogeochemical cycling of trace elements like selenium (Se) in the Arctic Ocean. This study described the first quantitative examination of the biogeochemical cycle of selenium in the Amerasian Basin, providing the baseline from which future changes can be identified. Aerosol, dissolved and particulate water samples were collected for Se determinations during the U.S. GEOTRACES GN01 Arctic expedition that sampled the two parts of the Amerasian Basin in 2015: The Makarov Basin on the way to the North Pole and the Canada Basin on the return trip to Dutch Harbor, Alaska.

Particulate Se concentrations were low throughout the cruise with the highest concentrations occurring at the bottom depths of the shallow shelf stations (0.06 nM). Particulate Se to particulate organic carbon atomic ratios were around phytoplankton ratios (~10^{-6}) on the shelf, but were elevated (10^{-5}) in the basin. Aerosol Se concentrations were low (0.01 – 0.11 nmol m^{-3}, n=13), but enrichment factors were elevated and ranged from 1540 to 66698, suggesting distant fossil fuel combustion or local gaseous sources such as marine biogenic release of dimethyl selenide as a dominant source of aerosol Se. Generally, the depth profiles of the dissolved Se species did not resemble those of nutrient-like profiles seen in other

ocean basins. Prediction of selenite and selenate concentrations using silicate and phosphate concentrations, shown to be accurate in other oceans, tended to overestimate selenate and underestimate selenite concentration throughout the Amerasian Basin. This lack of agreement suggests a slower than normal oxidation rate from selenite to selenate.

Estimated fluxes of total dissolved Se indicate that $1.0 \pm 0.5 \times 10^8$ mol Se enter and $1.0 \pm 0.1 \times 10^8$ mol Se leave the Amerasian Basin each year. The Atlantic Ocean is the dominant factor in both input and removal of water to and from the Arctic. Therefore, it likely plays a major role in the Se budget of the Arctic and future efforts should be made to directly measure the input and removal of Se via the Atlantic Ocean. The overlap in total input and removal fluxes suggest that the Se cycling in the Amerasian Basin is at steady state.

Due to the cycle being in steady state, residence times of Se were calculated throughout the basin. Selenium was calculated to have a total Amerasian Basin residence time of 149 ± 112 years and 151 ± 27 years by dividing the Se inventory by the total input rate and total removal rate respectively. Se in the intermediate basin layer, the basin water above the Lomonosov Ridge sill depth, had a residence time of 71 ± 22 years. These residence times are roughly 5 and 2 times longer than the residence time of the water highlighting the high rate of dissolved Se regeneration.

The Arctic Ocean will continue to change in response to a warming climate. Increased river discharge, smaller ice extent, and ice-free summers are likely to modify the biogeochemical behavior of trace elements in the Arctic and this study provides information on how the Se cycle might be affected.

ACKNOWLEDGMENTS

I am extremely grateful for Dr. Cutter's guidance throughout this entire project and for turning this Geologist into an Oceanographer.

TABLE OF CONTENTS

Page

LIST OF TABLES

Table Page

LIST OF FIGURES

Figure Page

CHAPTER 1

INTRODUCTION

The Arctic Ocean is a unique basin consisting of less than 5% of the total world ocean area, but receiving greater than 10% of the world river run-off (McClelland et al., 2008). The shelf to basin area ratio of the Arctic Ocean is the largest of all the ocean basins, with the shelf attributing up to 35% of the basin area (Kadko and Muench, 2005). The large shelf area is in part due to the enclosed nature of the basin. The Arctic Ocean is connected to the Pacific through the narrow and shallow Bering Strait, and the Atlantic via the narrow but deep Fram Strait, the shallow Barents and Norwegian Seas, and the shallow waters around the Canadian Archipelago. Isolation, coupled with ice covered conditions of the region, have deterred commercial exploitation of the Arctic Ocean (Hamilton, 2011). In the past, extensive sea ice covered vast regions of natural resources in the region. The Arctic has been estimated to contain 90 billion barrels of oil and 44 billion barrels of natural gas with 84% of the oil and gas expected to be offshore (Bird et al., 2008). Global warming has already caused dramatic reduction in the extent of Arctic sea ice that has led to increased exploration, tourist traffic, development, and shipping in the region (Reeves et al., 2014). Throughout history, natural environments receiving high human activity have been dramatically changed (Goudie, 2013), suggesting an increased human presence in the Arctic will change the region. Physical transformations of the Arctic Ocean are likely to change the biogeochemical cycling of Se in the Arctic. Continued global warming is likely to have a more severe and rapid effect on the Arctic Ocean than other ocean basins (Pachauri et al., 2014) and these changes are likely to alter the

cycling of trace elements in the Arctic. Reduced ice cover will allow increased sunlight, possibly promoting primary productivity and decreasing surface Se concentrations. Conversely, increased riverine discharge (Peterson et al., 2002) along with the warming of the surface waters from the removal of the sea ice could increase stratification due to a warmer fresher surface layer above colder, higher saline waters, decreasing primary productivity, resulting in higher Se surface concentrations. The anticipated increase in human activity will increase the chance of contamination by metals like mercury (Wang et al., 2004; Fisher et al., 2012), vanadium (Bourgoin and Risk, 1987), and selenium (Pacyna and Pacyna, 2001; Kavlak and Graedel, 2013). These potential changes to the selenium cycle in the Amerasian Basin will only be identified if there is a baseline cycle to which to compare it. This thesis provides the first assessment of the selenium cycle in the Amerasian Basin, allowing for future changes to be identified.

Selenium is a group 16 element with six valance electrons, an atomic number of 34, and an atomic mass of 78.96 u (Cotton and Wilkinson, 1988). The 6 valance electrons allow selenium to exist in oxidation states of -2, 0, +2, +4, and +6, making it most similar to sulfur (Meyer et al., 1992). Selenium has an electronegativity of 2.48 similar to sulfur (2.44), but lower than oxygen (3.44), both 6 valence electron elements (Cotton and Wilkinson, 1988). In biological systems, selenium is most commonly found in diselenides, selenols, and selenoethers (Meyer et al., 1992).

Selenium (Se) is both essential and toxic depending on the concentration and chemical speciation. Selenium is found in soils throughout the world, especially in sulfur deposits and in combination with lead, copper, and iron (Moxon et al., 1939). Sedimentary rocks of Cretaceous

formations are the highest Se-containing rocks (Moxon et al., 1939). The weathering of selenium-containing rocks and volcanic emissions are natural ways Se enters the ocean (McNeal and Balistrieri, 1989). At natural low nanomolar concentrations, selenium acts as an essential nutrient and is incorporated into selenoproteins (Ryan-Harshman and Aldoori, 2005) and antioxidant selenoenzymes (Steinbrenner and Sies, 2009). When concentrations are high, into the milimolar rage, Se is toxic and becomes carcinogenic (Spallholz, 1994), and increases the toxicity of arsenic (Sun et al., 2014). Selenium exists in multiple oxidation states, with Se(IV) being preferentially taken up over Se(VI) (Wrench and Measures, 1982; Riedel et al., 1996). Se(IV) is more toxic to both prokaryotic and eukaryotic cells due to sulfate metabolism being more effective on Se(VI) than Se(IV) (Shamberger, 1983; Rosen and Liu, 2009).

Selenium is an essential micronutrient for animals, functioning as antioxidants in the form of selenoproteins (Ryan-Harshman and Aldoori, 2005). In humans, selenium helps regulate immune functions as the selenoproteins selenocysteine and selenomethionine (Steinbrenner and Sies , 2009). Selenoenzymes incorporate selenium into the activation site to prevent unwanted oxidation in the body (Steinbrenner and Sies, 2009). Selenium is also used to remove toxins from the body. Selenium acts as a cofactor for glutathione peroxidases in the reduction of hydrogen peroxide (Lippard and Berg, 1994). At low levels, selenium will form an arsenic-selenium compound that is excreted extracellularly, decreasing the toxicity of arsenic (Sun et al., 2014). Selenium will also bind to mercury, removing the toxic effect of the element (Yoneda and Suzuki, 1997). The toxicity of cadmium(II) is neutralized by binding with hydrogen selenide in the body (Nuttall and Allen , 1984). Low levels of selenium have also been shown to have anticarcinogenic properties (Spallholz , 1994; Clark et al., 1996; Ganther, 1999).

Determining the biogeochemical cycles of trace elements, including selenium, in the present Arctic Ocean will provide a baseline of the biogeochemical cycles at work in the Arctic ecosystem. To date, there have been few ocean-scale studies of trace elements done in the Arctic. However, existing data show the usefulness of trace elements for revealing ocean processes in the Arctic Ocean. For example, knowing the cycling of barium, aluminum and silicate allowed deep-water circulation maps to be produced (Roeske et al., 2012). These earlier studies did not include many trace elements, preventing a comprehensive biogeochemical assessment of the Arctic Ocean. The Arctic selenium cycle described in this study, combined with the full complement of nutrients, physical transport, and other trace elements studied during the Arctic GEOTRACES project, provide an initial biogeochemical assessment of the Arctic Ocean required to identify any changes to the chemical health of the Arctic in the future. This thesis examined the qualitative and quantitative aspects of Se cycling in the Arctic Ocean.

Known Biogeochemistry of Selenium in the Ocean

Selenium can exist in several oxidation states (IV, selenite; VI, selenate; 0, elemental selenium; -II, selenide) and has particulate and dissolved forms within these oxidation states. Selenium speciation and distribution have been studied in the North Pacific (e.g., Cutter and Bruland, 1984; Rue et al., 1997), South Pacific (Sherrard et al., 2004), estuaries (e.g., Takayanagi and Wong, 1984; Measures and Burton, 1978; Cutter 1989a; Meseck and Cutter, 2006), Atlantic Ocean (e.g., Measures and Burton, 1980; Cutter and Cutter , 1995, 1998, 2001), and coastal waters (e.g., Wrench and Measures, 1982; Apte et al., 1986; Cutter and Cutter, 2004). A general biogeochemical cycle of selenium has been developed from these studies (Figure 1),

with prominent features being selective uptake of selenite over selenate by phytoplankton, reduction of dissolved selenium into particulate organic selenide inside phytoplankton, a multi-step regeneration from particulate organic selenide to dissolved organic selenide, and a slow oxidation of all selenium species to dissolved selenate, the thermodynamically stable form of selenium in the oxic ocean (Cutter and Bruland, 1984). The first vertical profiles of selenite and selenate in the Pacific Basin were done by Measures et al. (1980) while the vertical profiles in the Atlantic Basin were done by Measures and Burton (1980). Both basins showed that selenite followed the uptake and regeneration pattern of silica and phosphate, while selenate followed that of phosphate, with surface depletion and regeneration with depth. Measures et al. (1980) were able to use the relationship selenite and selenate have with silica and phosphate to predict selenium concentrations. The method worked for both Atlantic and Pacific profiles. Three years later, Measures et al. (1983) showed that the nutrient-like behavior of the selenite and selenate vertical profiles also existed in the Indian Ocean and that departures from the normal vertical profiles of selenite and selenate could be attributed to the dissimilatory reduction of these oxidized Se species within the oxygen minima zones.

Atmospheric deposition is a major component in the marine selenium cycle (Cutter and Bruland, 1984; Cutter, 1993; Cutter and Cutter, 1998). Atmospheric deposition in the northern Pacific Ocean is dominated by sporadic dust events and increases with latitude (Uematsu et al., 1985). Mosher et al. (1987) found that aerosol samples collected from the high-latitude North Pacific had much higher Se concentrations (0.25 ± 0.16 ng m^{-3}) than any of the mid or lower latitude sites (0.10 ± 0.05 ng m^{-3}; Mosher et al., 1987), supporting the findings of Uematsu et al., 1985.

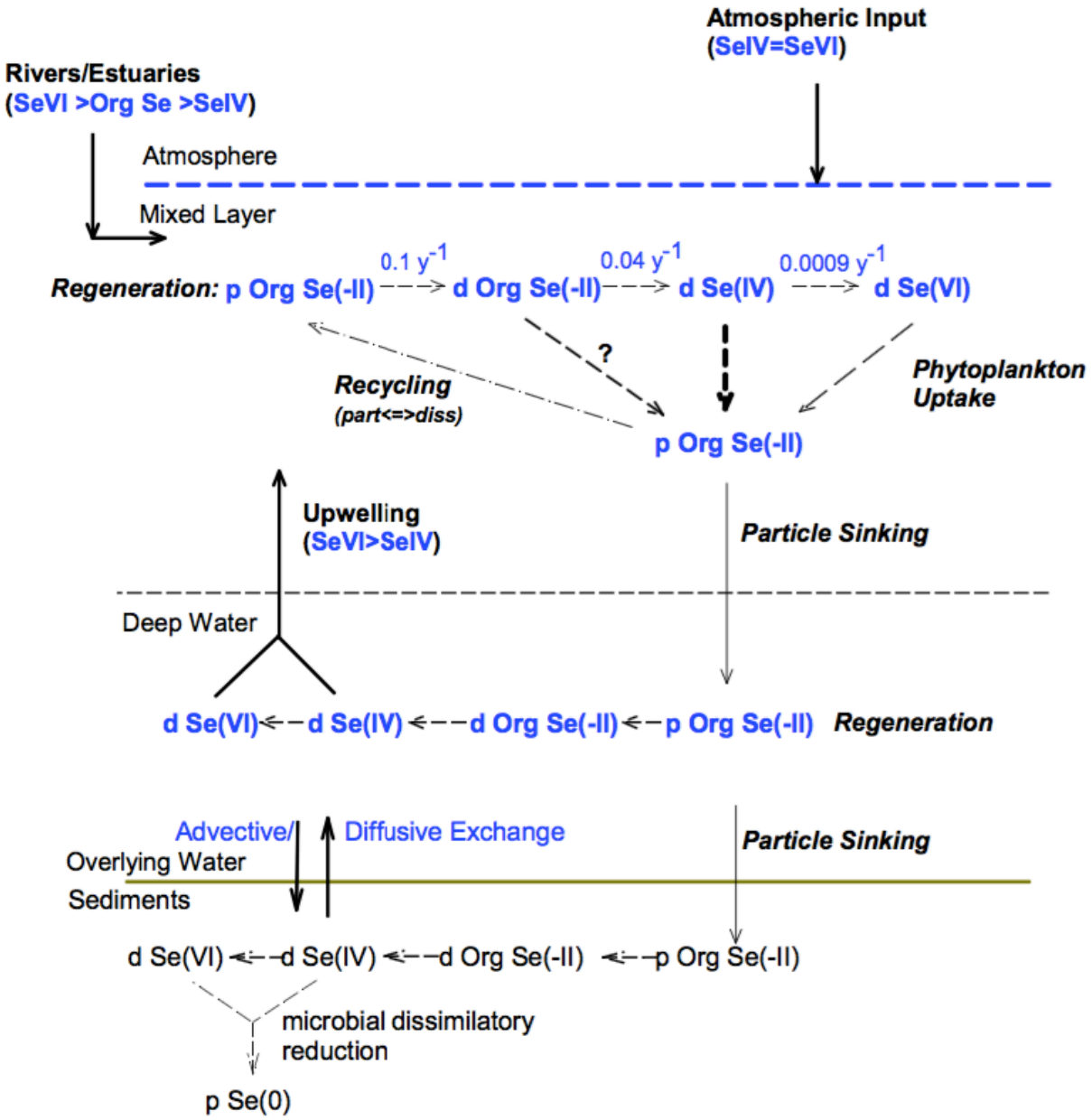

Fig. 1. An overview of the biogeochemical cycling of selenium in an ocean. ("p" = particulate, "d" = dissolved). Solid arrows indicate fluxes and dashed arrows are pathways of transformation with the thickness of an arrow indicating the relative size of the pathway. Selenium species inside the parenthesis indicate the relative species concentration for that input method. First order rate constants for the multistep regeneration of particulate to dissolved selenium species are listed above the dashed arrows. Adapted from Cutter and Bruland, (1984).

This trend of higher latitude sites having higher aerosol deposition of selenium was further supported by a 2001 cruise from Japan to just south of the Bering Sea to Hawaii where

Ranville et al. (2010) found that total dissolved selenium concentrations in surface waters showed a general correlation with aerosol deposition and increased with increasing latitude (r^2=0.46). Recent studies in the North Pacific identified atmospheric deposition of selenium originating from eastern Asia, likely from the extensive coal combustion in the area (Lovvorn et al., 2013; Ranville et al., 2010; Mosher et al., 1987). Aerosol samples along with surface water samples could provide evidence for or against the continuation of this eastern Asian air mass into the Arctic Ocean. Although significant work has been done studying selenium throughout the world's oceans, selenium speciation and distributions in the Arctic Ocean have not been examined to date.

Physical characteristics of the Arctic Ocean

The Arctic Ocean is split into 4 major basins: Canada, Makarov, Amundsen, and Nansen. The Canada and Makarov make up the Amerasian Basin, and the Amundsen and Nansen combined form the Eurasian Basin (Jakobsson et al., 2008); these are surrounded by half a dozen Arctic "Mediterranean" seas (Aagaard et al., 1985; Figure 2). The Lomonosov Ridge separates the Amerasian Basin in the west from the smaller Eurasian Basin in the east (Jones et al., 1995). The Amerasian Basin is split by the Alpha-Mendeleyev Ridge into the Canada and Makarov Basins (Rudels, 2009). The sources of seawater for the Arctic Ocean come from the Atlantic through the Barents Sea, the Norwegian Sea, and the Fram Strait, and the Pacific through the Bering Strait (Fig. 2; Jones et al., 1998).

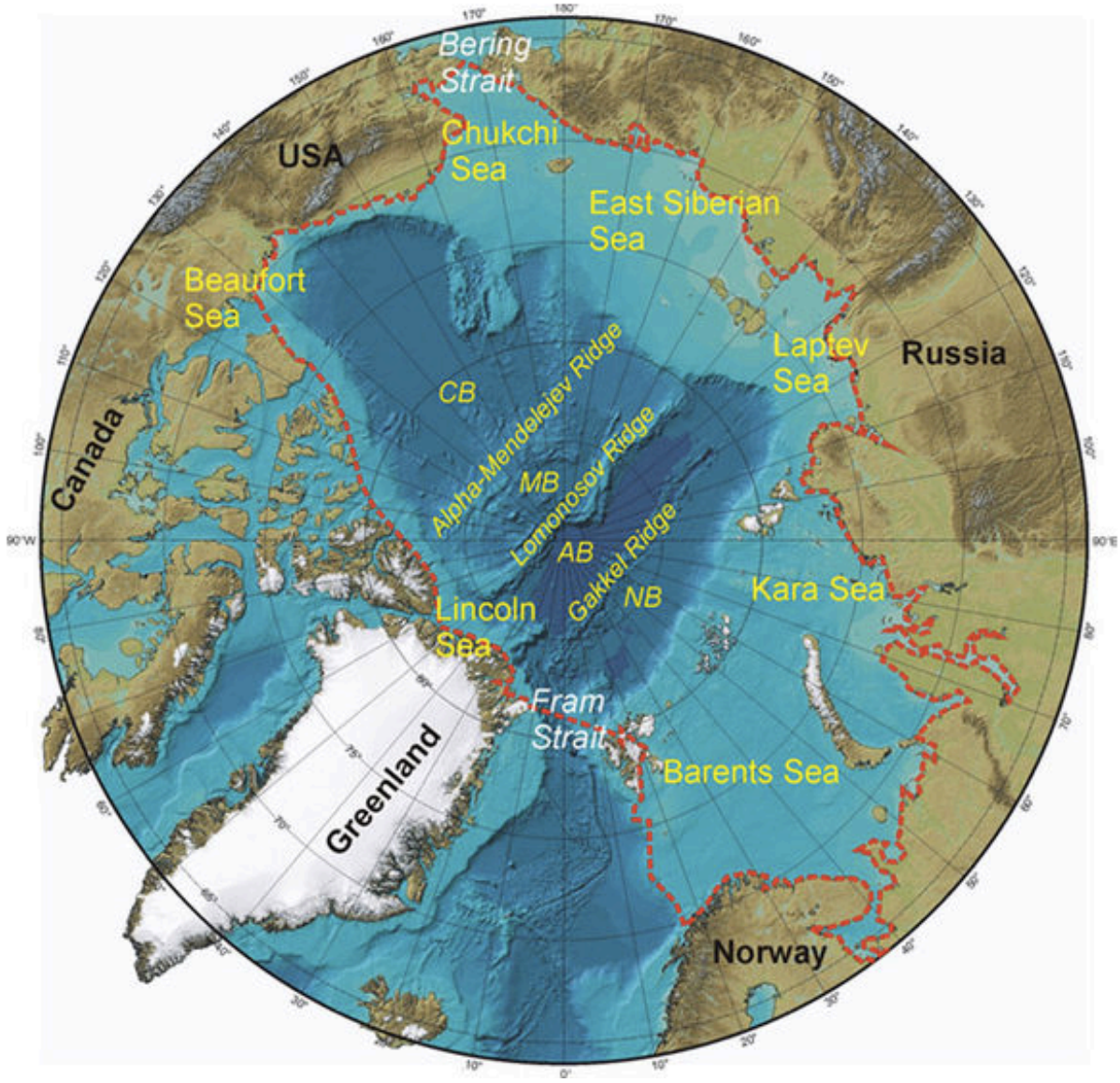

Fig. 2. The basins and seas of the Arctic Ocean generated from the International Bathymetric Chart of the Arctic Ocean (Jakobsson et al., 2008). CB = Canada Basin, MB = Makarov Basin, AB = Amundsen Basin NB = Nansen Basin. The red dots indicate the extent of the Arctic Ocean.

The Bering Strait is shallow, reaching a maximum depth of 50 m (Woodgate, 2017). Therefore, only shallow Pacific Ocean water enters the Amerasian Basin, causing the Atlantic Ocean to be to the dominant source of sea water in the Arctic. Continual freshwater input from rivers and seasonal input from the summer ice melt maintain a fresh surface layer, ensuring

stratification and limiting vertical mixing in the Arctic Ocean (McLaughlin et al., 2004). Mixing is further limited by a prevalent cold halocline between 50 and 200 m throughout the Arctic Ocean (Aagaard et al., 1981; Morison et al., 1998). Pacific Water is the dominant source for surface water in the Canada and Makarov Basins, while in the Eurasian Basin, Atlantic Water is the dominant source (Jones et al.,1998). The deep water of the Arctic Ocean is Atlantic in origin, with Pacific origin water reaching a maximum depth of 500 meters (Aagaard, 1981, Swift et al., 1997; Jones et al., 1998). Despite their proximity to the Pacific Ocean, the deep water in the Canada and Makarov Basins is Atlantic in origin, with the deep water inflow coming from the Eurasian Basin (Swift et al., 1997).

The identity of source water directly affects the expected concentrations of selenium. If selenium was conservative in the Arctic Ocean, the water above the halocline near the Bering Strait would have selenium concentrations similar to those of the Pacific Ocean. This selenium signature would look more like the Atlantic Ocean the farther away from the Pacific source the sample was taken. Water dominated by a Pacific Ocean source is, excluding anomalous mid-depth eddies mixing across the halocline (Swift et al., 1997), restricted to above the cold halocline and reaching a maximum depth of 250 meters. Selenium does not behave conservatively in other oceans so it is unlikely to be conservative in the Arctic Ocean. Therefore, Se concentrations may be different than the source concentration, requiring high resolution sampling and utilization of other tracers to clearly identify Se sources.

Riverine input has the potential to be an important source of Se to the Amerasian Basin. The Arctic Ocean consists of less than 5% of the total world ocean area, but receives greater than 10% of the world river run-off (McClelland et al., 2008). Unfortunately, previous Arctic

expeditions have not sampled Se in Arctic rivers. Cutter (1989b) compiled the available selenium data for the rivers around the world. Ignoring highly contaminated rivers where concentrations are much higher than the average, like such as San Luis Drain Canal with an average concentration of 3040 nM, the average total dissolved Se concentration in rivers around the world was 1.8 ± 1.5 nM (n=28). The disproportionally high riverine input to the Arctic could translate into a significant freshwater source of dissolved selenium species to this basin if concentrations are substantially above the 1.8 nM world average.

Amerasian Basin Water Masses

Rudels (2009) describe five distinct water masses in the Amerasian Basin: Polar Mixed Layer (PML), Halocline, Atlantic layer, Intermediate, and Deep. Each of these water masses are defined by a density range and exhibit unique circulation characteristics and will be described in ascending density. The PML is identified by its low salinity, between 30 and 32.5, and typically consists of the upper 50 meters. The PML generally circulates in an anticyclonic motion around the Amerasian Basin (Figure 3). The halocline layer is defined as having a potential temperature near freezing and a salinity between 32.5 and 34.5. The halocline layer is 100 – 250 m thick and has a cyclonic flow around the Amerasian Basin (Figure 4). The Atlantic Layer has a potential temperature above 0 ^{o}C, with a salinity between 34.5 and 35. The Atlantic Layer is 400 – 700 m thick with a cyclonic circulation around the Amerasian Basin (Figure 5). The Intermediate water sits directly below the Atlantic layer, but above the Lomonosov Ridge, with a potential temperature between -0.5 and 0 ^{o}C and a salinity between 34.87 and 34.92. The intermediate water travels around the Amerasian Basin in a cyclonic flow (Figure 5). The deep water is

defined as having a potential temperature between -0.55 and -0.5 ^{o}C and a salinity between 34.92 and 34.96. The deep water in the Amerasian Basin is isolated by the Lomonosov Ridge, with an average ventilation time of 700 years (Ostlund et al., 1987).

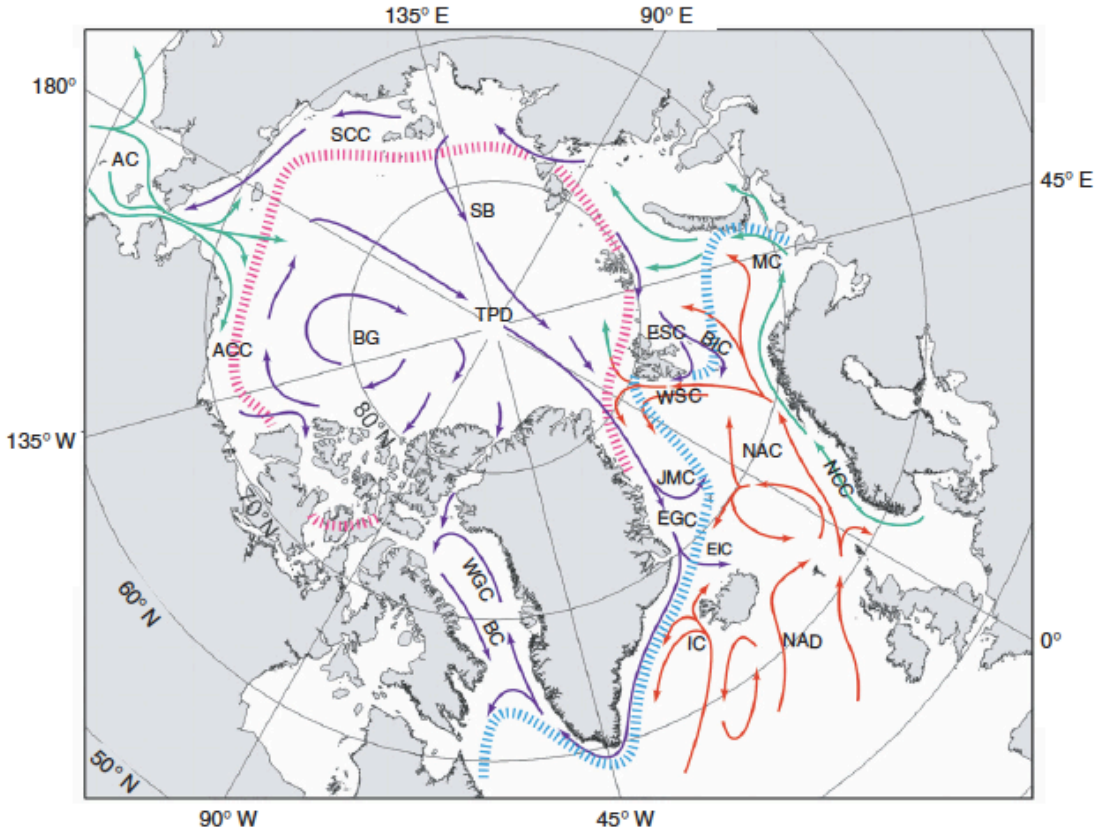

Fig. 3. Polar Mixed Layer circulation of the Arctic Ocean. Described by Rudels (2009).

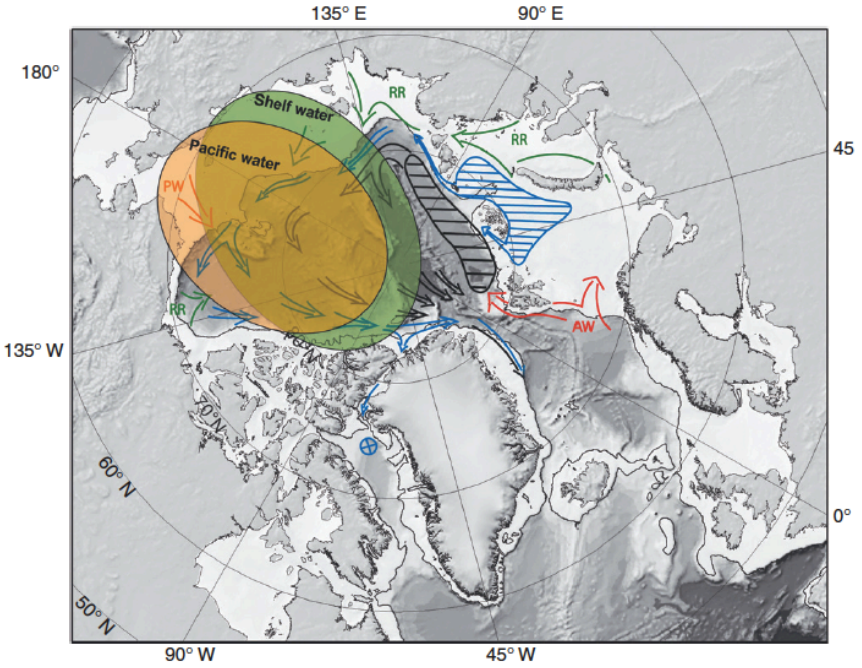

Fig. 4. Halocline circulation of the Arctic Ocean. Based on Rudels et al (2004), as published in Rudels (2009)

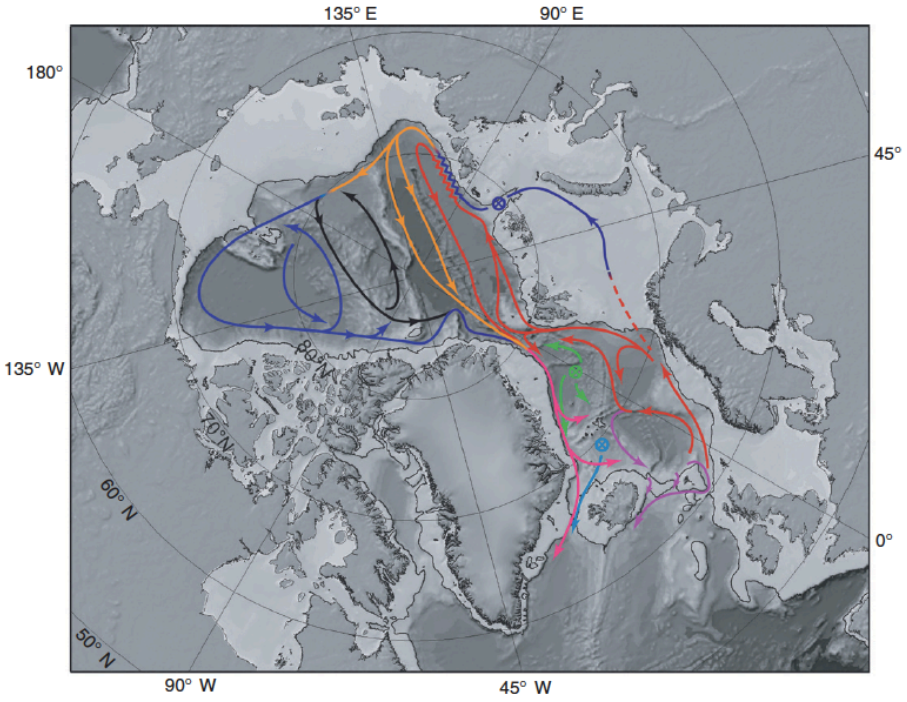

Fig. 5. Circulation pattern of the Atlantic and Intermediate water masses of the Arctic Ocean. First described in Rudels et al., (1994). Image taken from Rudels (2009).

Research approach

The goal of this study was to quantitatively reveal the biogeochemical cycling of Se in the Amerasian Basin and compare it to previous reports for selenium cycling in the Pacific and Atlantic Oceans. In order to achieve this goal, selenium concentrations and speciation were determined across a transect through the Amerasian Basin (Figure 6). Fluxes of Se into and out of the Amerasian Basin were quantified by determination of the concentration, and distribution of dissolved, particulate, and aerosol selenium, then multiplying the determined concentrations by volume fluxes. The combination of fluxes and internal cycling allowed for the mass balance of Se in the Amerasian Basin to be constructed.

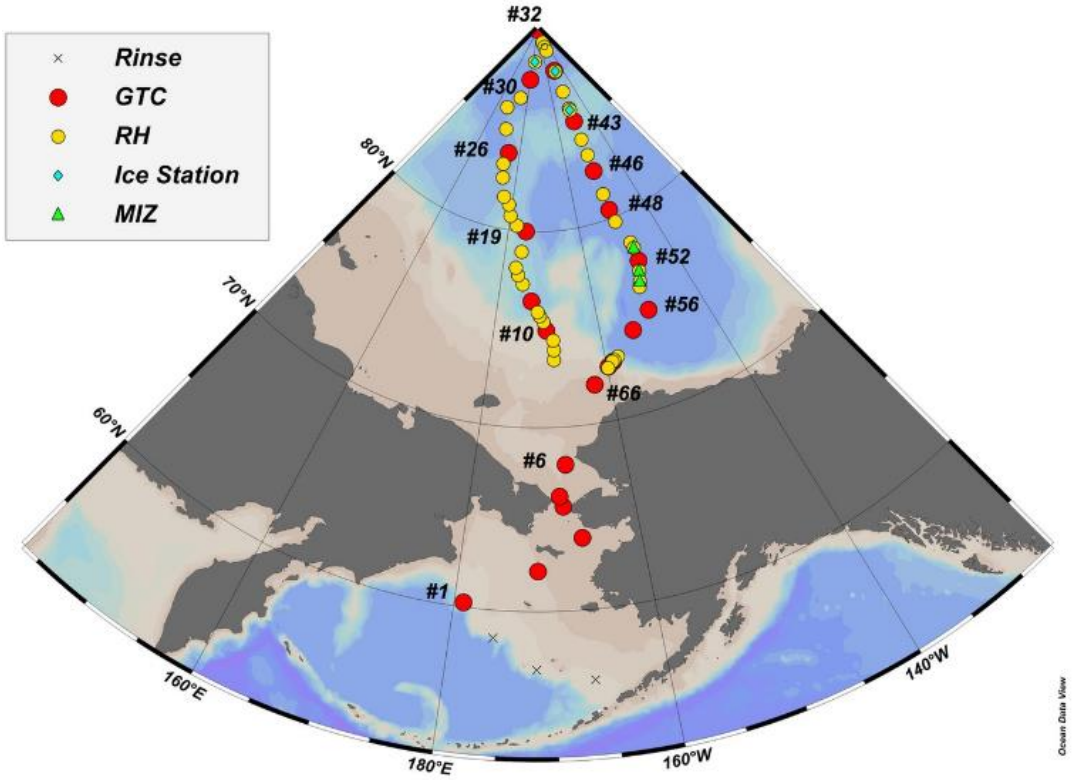

Fig. 6. Cruise transect from Dutch Harbor, AK, to the North Pole going north through the Makarov basin (stations 1-32) and south return to Dutch Harbor, AK, through the Canada basin (stations 33-66). Map generated by Mariko Hatta, University of Hawaii.

CHAPTER 2

SAMPLING AND ANALYTICAL METHODS

Sample Collection

Dissolved, particulate, and aerosol samples were taken at 15 stations throughout the U.S. Arctic Ocean GEOTRACES GN01 transect (Fig. 6). The dissolved samples were collected using the US GEOTRACES Trace Element Carousel (Cutter and Bruland, 2012) to insure clean samples. To minimize contamination, the carousel was equipped with twenty-four 12 L GO-FLO bottles, titanium housing for all electronics, and lowered on a Vectran conducting cable that ran through nonmetallic sheaves (Cutter and Bruland, 2012). The GO-FLO bottles were triggered while the carousel was moving upward at a speed of 3 m min^{-1}. The dissolved samples were filtered through 0.4 µm membrane filters and into 1 L borosilicate glass bottles, then acidified to a pH less than 1.8 with HCl. The sample bottles were stored in in the dark at ambient lab temperature until analyzed within 12 months of collection at the Cutter Lab at Old Dominion University. Particulate samples were collected by Dr. Lam at the University of California, Santa Cruz on 0.8 µm Supor filters using in situ McLane pumps at various depths (Bishop et al., 2012). The pumps were suspended at targeted depths for four hours while the McLane pumps filtered water through the 0.8 µm Supor filters. The volume of water that passed through each filter was recorded by the pumps. The filters were frozen and stored at -80 ^{o}C until analyzed at Old Dominion University within 18 months of collection. Aerosol samples were collected by Dr. Marsay of the Buck Lab at Skidaway Institute of Oceanography continuously along the transect according to the methods established in Morton et al. (2013). The aerosol samples were

collected on 47 mm diameter Whatmann 41 filters using a high-volume aerosol sampler deployed above the ship's bridge. The filters were pre-cleaned with a 0.5 M HCl soak and rinsed with ultra-high purity water then dried in a laminar flow hood. The pumps only turned on when the wind speed was >0.5 m s^{-1} and blowing from ± 60 degrees from the ship bow for at least five continuous minutes to minimize the potential for contamination from the ship's exhaust stack. Samples were frozen and stored at -80 ^{o}C until analyzed at Old Dominion University within 18 months of collection. This Se study also analyzed surface sediments from 3 cores, multi-cores 6 and 8 and box core 4, on the Alaskan Shelf taken during the 2005 HOTRAX expedition (Table 1; Darby et al., 2009).

Analytical Methods

Dissolved selenium speciation and concentrations were determined on stored samples using the hydride generation methods described in detail in Cutter (1978, 1982, and 1983). For selenite determination, a water sample in a glass stripping vessel was acidified to 4 M HCl. Helium gas was bubbled through the acidified solution, through a -60 ^{o}C U-tube to remove water vapor, and then through a glass U-tube packed with silanized glass wool, immersed in liquid nitrogen. A borohydride solution was added, then the sample was stripped for 10 minutes to collect hydrogen selenide. After removing the trap from the liquid nitrogen, hydrogen selenide was released in a concentrated burst to the atomic absorption spectrometer fitted with a quartz tube burner and air-hydrogen flame, which detected the peak of hydrogen selenide. The area under the peak was determined, the area of the blank samples was

subtracted from the area of the sample, and the resulting area was converted to a selenium concentration using the slope of a standard additions of selenite calibration curve.

Table 1. Latitude and Longitude of the sampling stations (S= sample stations), and median locations of aerosol samples (A=aerosol samples) collected during the 2015 U.S. GEOTRACES Cruise. Location of sediment cores, B=Box core, MC=multi-core, collected during the 2005 HOTRAX expedition.

Type	Latitude (^{o}N)	Longitude (^{o}W)
A1	65.05	170.30
A2	77.36	173.53
A3	81.88	175.00
A4	85.14	174.58
A6	89.18	170.97
A7	88.01	149.71
A8	85.92	149.71
A9	83.19	150.00
A10	79.88	149.00
A11	76.75	149.00
A12	74.65	152.00
A13	73.15	158.25
A14	63.00	164.50
B4	72.21	157.09
MC6	72.69	157.32
MC8	71.63	156.88
S1	60.18	179.12
S2	62.27	171.65
S3	64.05	166.90
S4	65.81	168.62
S6	67.99	168.10
S9	74.50	168.85
S10	75.00	170.56
S12	75.78	171.23
S19	80.00	174.96
S30	87.52	179.81
S43	85.14	150.10
S48	80.43	149.43
S51	78.17	147.86
S57	73.36	156.81
S60	73.00	158.85
S61	72.80	159.62
S66	72.04	162.58

Selenate and total selenium determinations require an additional boiling step before the hydride generation procedure. Selenate determinations involved boiling a sample that was acidified to 4 M HCl for 15 minutes and left to sit overnight before the hydride procedures were performed. The resulting concentration determined by the atomic absorption spectrometer was selenite + selenate. Subtraction of the selenite concentration yielded the selenate concentration. Total selenium determination required the addition of potassium persulfate solution to a sample acidified with HCl and boiled for 60 minutes. The hydride generation and stripping procedures and standard additions method of calibration yielded a selenium concentration representing the total of selenite + selenate + organic selenide. Subtraction of the selenite + selenate value from the total selenium concentration gave the concentration of organic selenide. The average detection limit for dissolved Se species was 0.04 nM (3σ, n=50). Precision from triplicate determinations was better than 10% (RSD, n=160). Accuracy for dissolved determinations was assured by the use of the standard additions method of calibration.

Water column particulate, aerosol, and sediment samples require an acid-digestion step to convert them to dissolved samples. This preparation generally followed the nitric-perchloric acid reflux digestion procedure put forth by Cutter (1985). The in situ pump or aerosol filters, or weighed amounts of dried sediment, were placed in Teflon digestion tubes, then acidified with 15 mL of concentrated HNO_3 and 20 pipette drops of 70% perchloric acid before going through two complete 25 minute digestions at 170 ^{o}C on the CEM Mars Microwave Digestion System. HNO_3 and perchloric acid were added at the beginning of each run. After the second digestion, the sample solutions were transferred to nitric-cleaned 50 mL glass beakers rinsing

the Teflon digestion tubes with DDI three times. The sample solutions were then slowly evaporated to near dryness, making sure not to burn or char the sample, then 10 mL of 6 M HCl was added to the solution to dissolve the residues. The solution was then poured into 9 cm Poly-Prep Chromatography Columns containing 4 cm of 106-180 µm mesh Bio RAD AG1x8 resin to remove iron that interferes with the hydride method. The solution that passed through the resin was collected in 30 ml precleaned polyethylene bottles. Once the digestion solution passed through the resin, the glass beakers were rinsed 3 times with 2-3 mL of 6 M HCl and poured into the column. Each rinse waited until the sample completely passed through the resin before the next rinse began. After rinsing was complete, the resin columns were flushed with 5 mL of 6 M HCl, which was also collected by the polyethylene bottles. After being poured through the resin, the samples were ready to be analyzed following the same procedure for total dissolved selenium analysis. The detection limit for total particulate Se, assuming an average filtration volume of 24 liters, was 7.8×10^{-4} nM, with an accuracy of 85% recovery of the BCR 277R estuarine standard (3σ, n=19). The precision for total particulate selenium based on triplicate analyses averaged 11% relative standard deviation to the mean.

Phosphate and silicate concentrations were determined by the Ocean Data Faculty group at the Scripps Institution of Oceanography on a Seal Analytical continuous-flow AutoAnalyzer 3. Phosphate analysis was determined using a modification of the Bernhardt and Wilhelms (1967) method. Phosphomolybdic acid, created by the addition of acidified ammonium molybdate to the sample, was reduced to phosphomolybdous acid as a result of the addition of dihydrazine sulfate. The sample was then passed through a 10mm flow cell and the absorbance was measured at 820 nm. Silicate analysis was performed using the method

described in Armstrong et al., (1967). Silicomolybdic acid, produced by the addition of acidified ammonium molybdate to the seawater sample, was reduced to silicomolybdous acid as a result of the addition of stannous chloride. The sample was then passed through a 10 mm flow cell and measured at 660 nm (www.scripps.ucsd.edu/ships/shipboardtechnicalsupport/odf/documentation/nutrient-analysis).

Error Propagation

Error was propagated when multiplying and averaging values with errors using the equation (Taylor, 1997):

$$\delta Q/Q = \text{sqrt}((\delta a/a)^2 + (\delta b/b)^2 \ldots (\delta z/z\delta)^2) \quad (1)$$

where δ is the error associated with the value, Q is the final value and a through z are the individual values being multiplied with their associated error. Uncertainties associated with literature values were assumed to be standard deviations if not otherwise specified. Equation 1 generated uncertainties as a percentage of the value. These percentages were then applied to the resulting value in order to present the uncertainty as values ± from the mean.

CHAPTER 3

SELENIUM DISTRIBUTIONS AND SPECIATION IN THE AMERASIAN BASIN

The dissolved, particulate, and sediment selenium data will be presented zonally starting with the shelf, then slope, then basin stations. The aerosol samples do not easily fit into these zones due to long collection times; therefore, atmospheric data are addressed separately.

Chukchi Shelf

Stations 2, 3, 4, 6, 61, and 66 were located on Bering Sea Shelf, and the Chukchi Shelf just north of the Bering Strait, and off the North coast of Alaska (Fig. 6; Table 1). Total dissolved selenium is relatively constant at Stations 3, 61, and 66, but does show an increase with depth at Stations 2, 4, and 6 (Figures. 7-12). Selenite decreases with depth before increasing at the bottom depth at Stations 2 and 6 (Figs. 7, and 10). Both selenite and selenate have nutrient-like profiles, surface depletion with regeneration and increasing concentration with depth at Station 61, with selenate also having a nutrient-like profile at Station 2. The macronutrients silicate and phosphate showed slight (Station 66; Fig. 12) to significant (Station 61; Fig. 11) increase in concentration with depth throughout the shallow shelf.

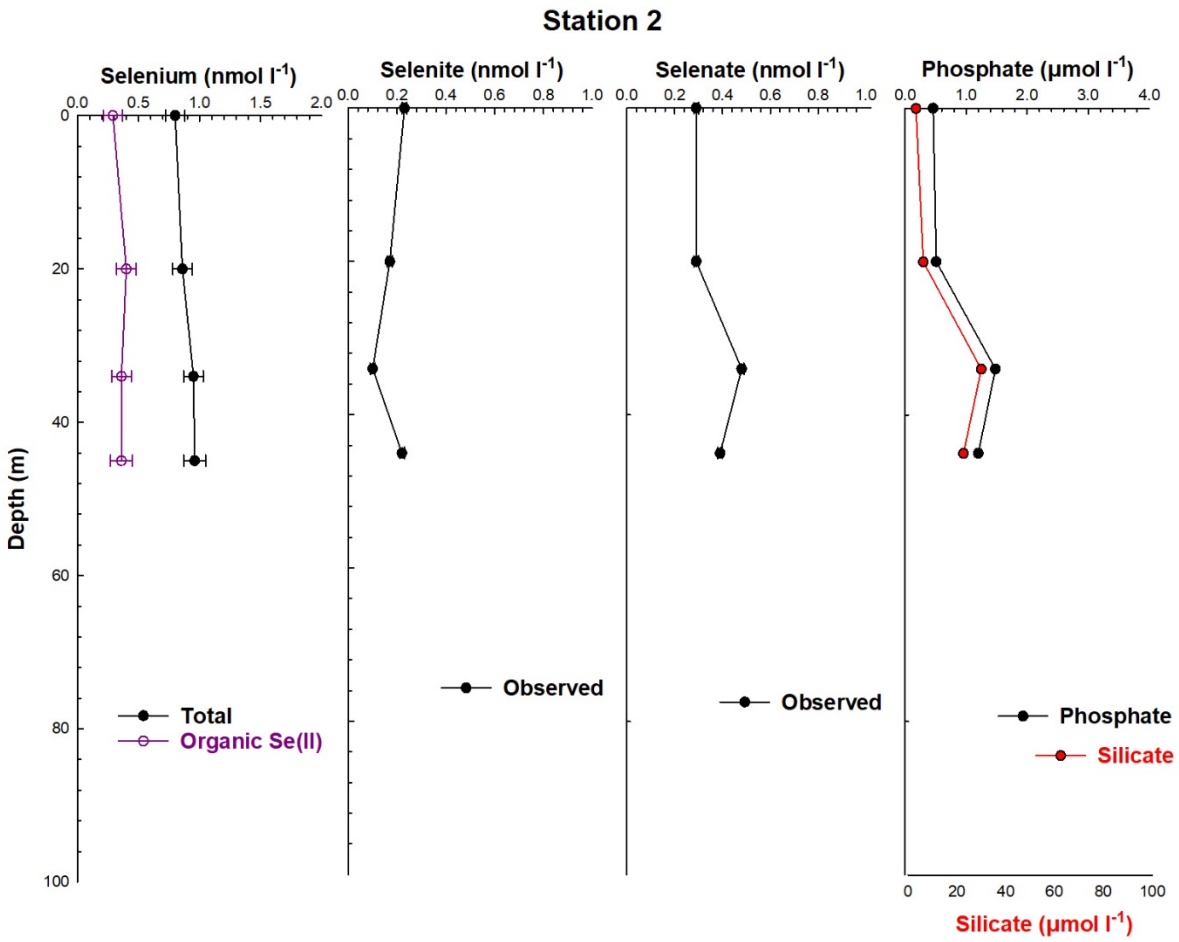

Fig. 7. Depth profile of dissolved organic selenide, selenite, selenate, and total selenium, as well as phosphate and silicate at Station 2. Error bars as standard deviations for concentrations are shown unless they are smaller than the symbols.

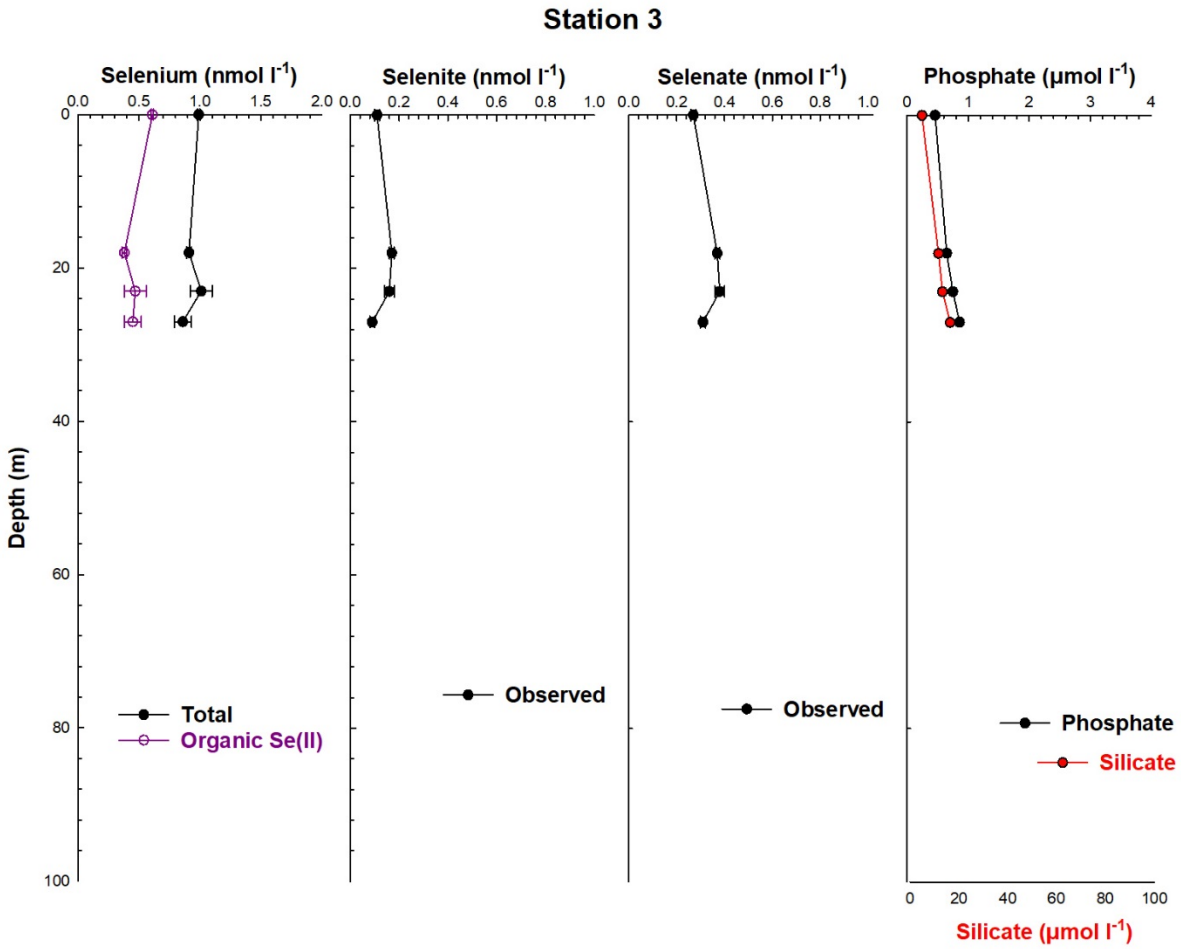

Fig. 8. Depth profile of dissolved organic selenide, selenite, selenate, and total selenium, as well as phosphate and silicate at Station 3. Error bars as standard deviations for concentrations are shown unless they are smaller than the symbols.

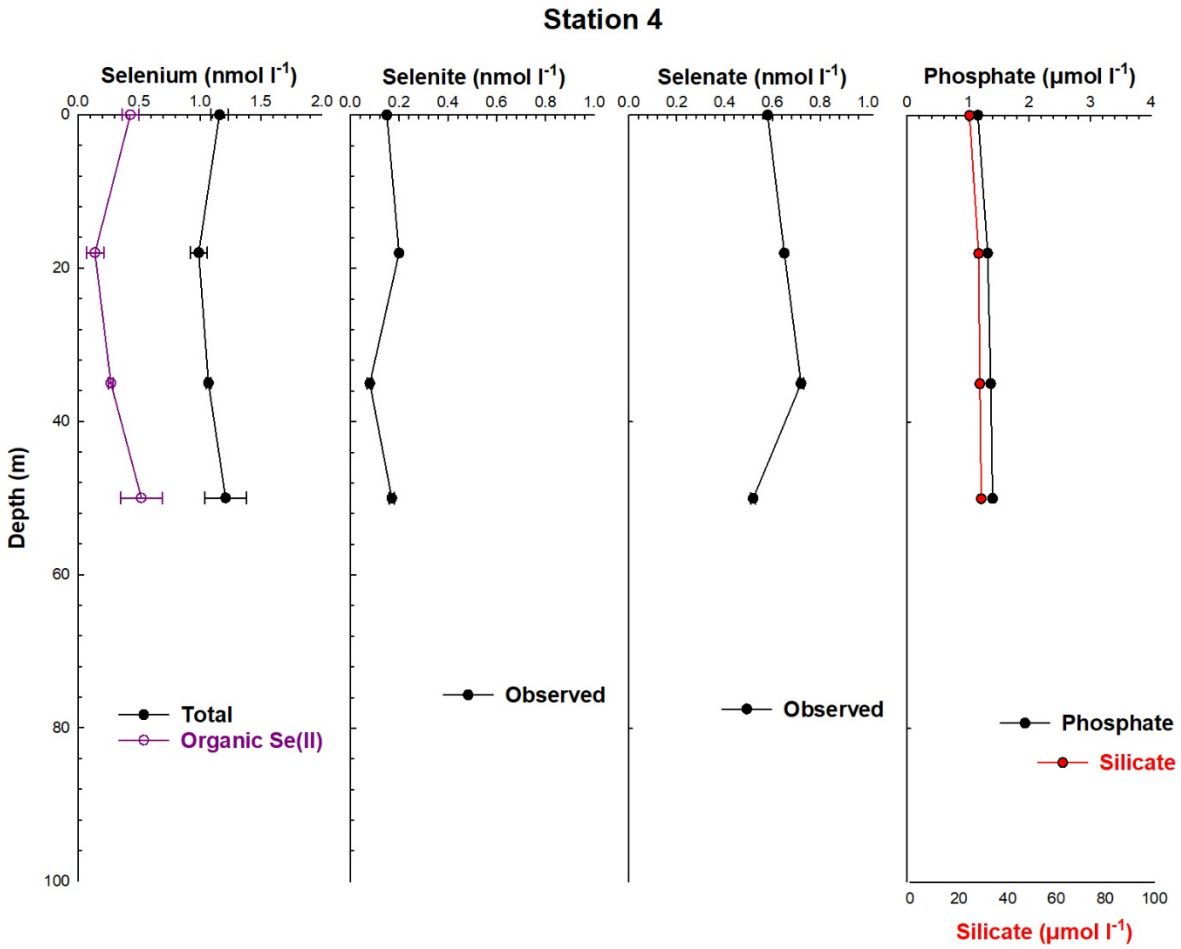

Fig. 9. Depth profile of dissolved organic selenide, selenite, selenate, and total selenium, as well as phosphate and silicate at Station 4. Error bars as standard deviations for concentrations are shown unless they are smaller than the symbols.

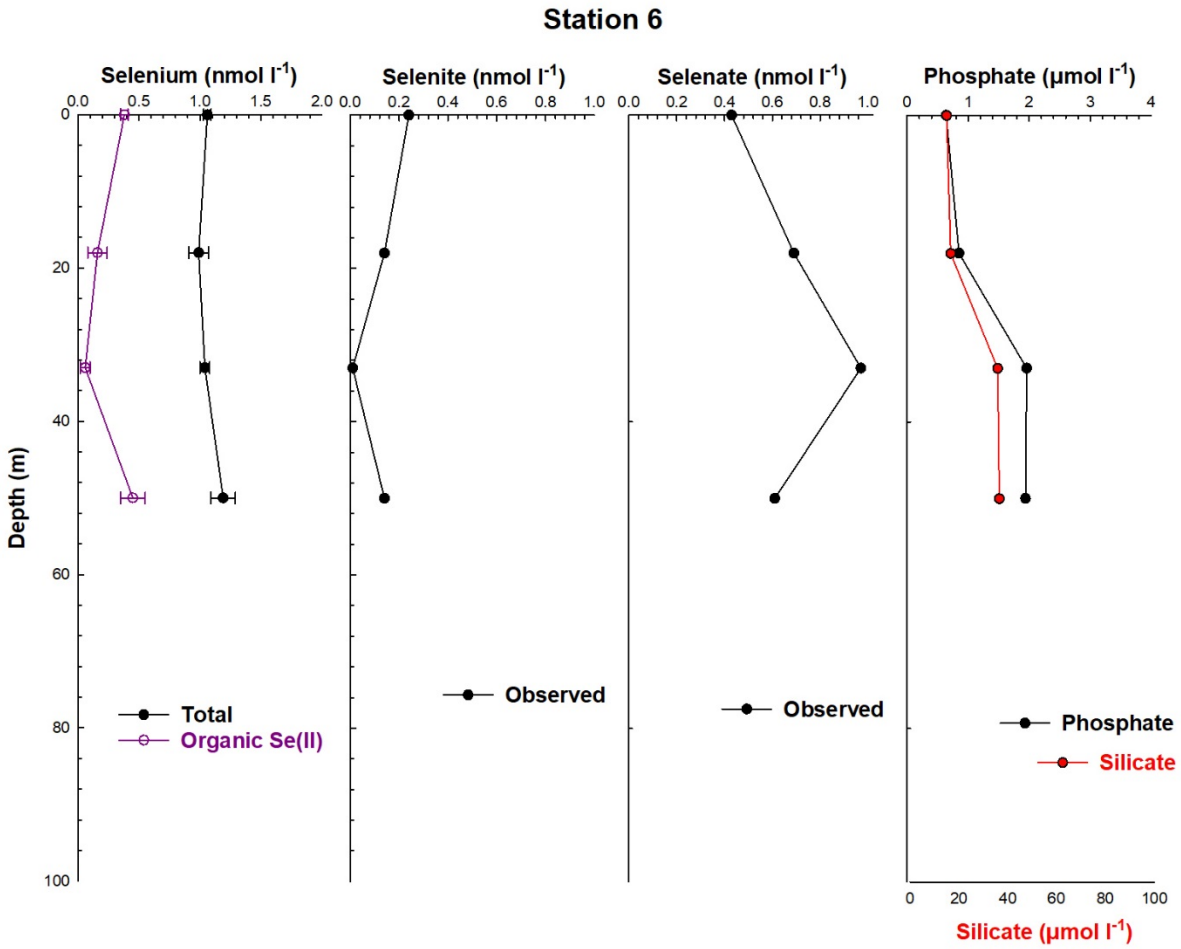

Fig. 10. Depth profile of dissolved organic selenide, selenite, selenate, and total selenium, as well as phosphate and silicate at Station 6. Error bars as standard deviations for concentrations are shown unless they are smaller than the symbols.

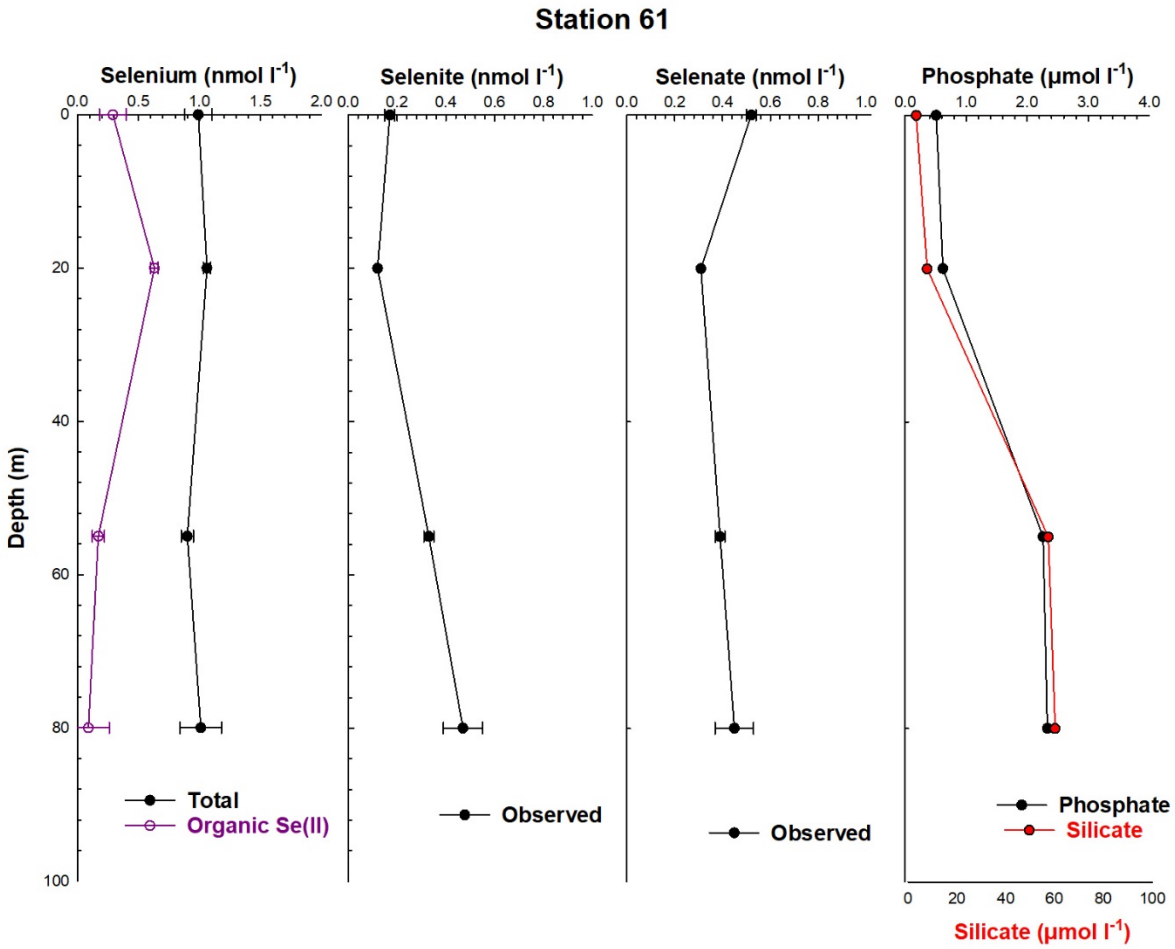

Fig. 11. Depth profile of dissolved organic selenide, selenite, selenate, and total selenium, as well as phosphate and silicate at Station 61. Error bars as standard deviations for concentrations are shown unless they are smaller than the symbols.

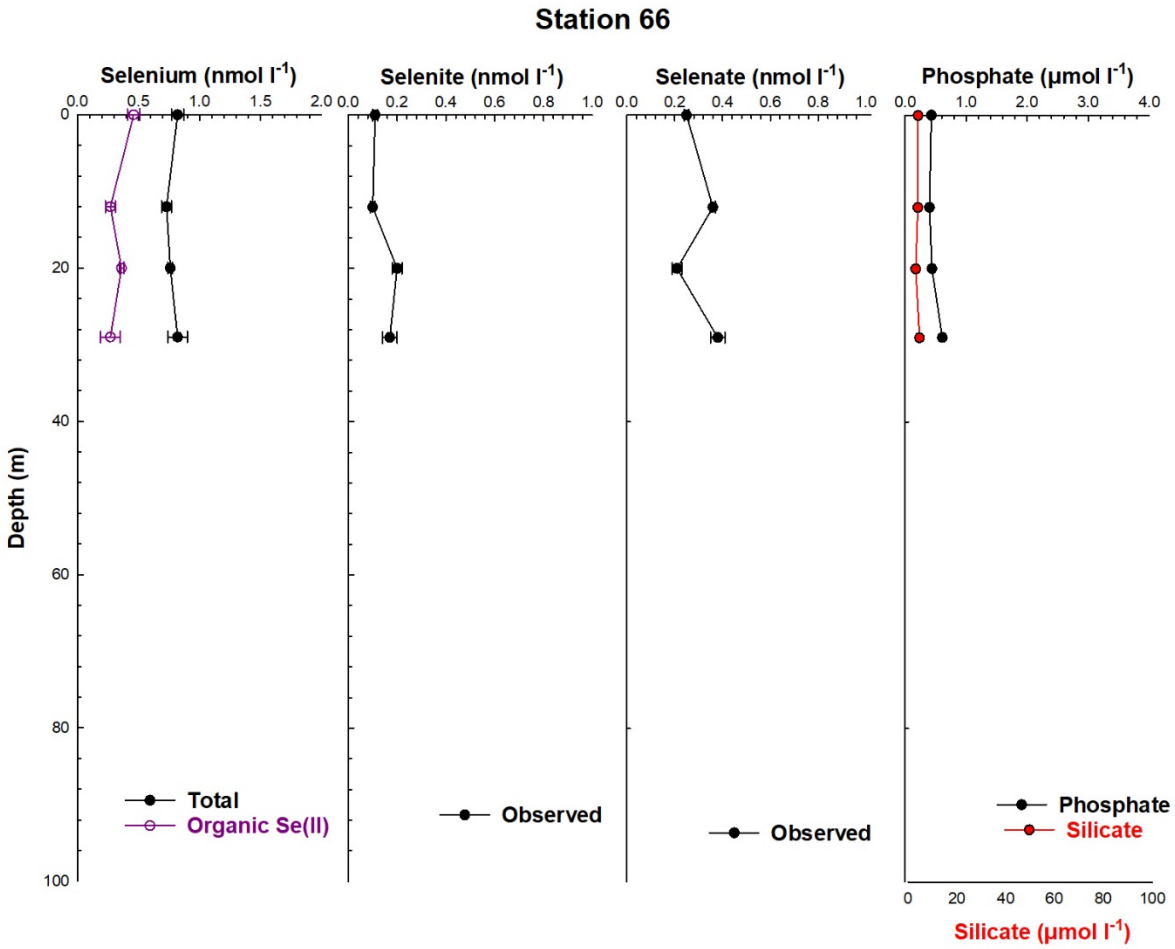

Fig. 12. Depth profile of dissolved organic selenide, selenite, selenate, and total selenium, as well as phosphate and silicate at Station 66. Error bars as standard deviations for concentrations are shown unless they are smaller than the symbols.

The depth-integrated-average (DIA) for each station was determined using the equation:

$$DIA = H * \sum ((C_n + C_{n+1})/2)*(z_{n+1} - z_n) \quad (2)$$

Where C_n, C_{n+1}, z_n and z_{n+1} are the concentration and depth at location n and n+1, respectively. Location n+1 was always the next deepest sampling depth after depth location n. H was the depth range in question. For the basin and slope stations, the DIA calculations were split into different ranges to avoid averaging across different water masses. The shelf stations, however,

were very shallow (<100 m) and therefore assumed to be all one water mass. The shelf stations had a mean DIA total Se concentration of 0.95 ± 0.11 nM (n=24; Table 2), with the highest DIA concentration at Station 4 in the Bering Strait (1.1 nM) and decreasing concentrations on either side of the strait by 12% to the South and 8% to the North.

Table 2. Depth integrated average (DIA) concentrations for organic selenide, selenite, selenate and total dissolved selenium at the shelf Stations and the average of each species for the shelf. n is the number of samples used in the DIA calculation.

Stations	Org. Se (nM)	Selenite (nM)	Selenate (nM)	Total Se (nM)	n
2	0.36 ± 0.05	0.17 ± 0.06	0.34 ± 0.09	0.89 ± 0.07	4
3	0.48 ± 0.10	0.14 ± 0.04	0.34 ± 0.05	0.95 ± 0.07	4
4	0.29 ± 0.17	0.17 ± 0.50	0.52 ± 0.09	1.1 ± 0.10	4
6	0.12 ± 0.16	0.13 ± 0.09	0.62 ± 0.24	1.0 ± 0.18	4
61	0.33 ± 0.15	0.26 ± 0.15	0.39 ± 0.09	0.92 ± 0.07	4
66	0.34 ± 0.15	0.14 ± 0.05	0.29 ±0.07	0.73 ± 0.08	4
Average	0.33 ± 0.09	0.17 ± 0.05	0.42 ± 0.13	0.95 ± 0.11	24

Particulate Se (pSe) concentrations were highest on the shelf (Figures 13 and 14) with the bottom depths at Stations 6 and 61 having the highest concentrations (0.05 nM; Figure 15). Of the water column inventories of selenium, pSe represented at most 5% and often less than 1% of the dissolved, which was lower than abundances seen in the San Francisco Bay (8.3 ± 2.6%; Doblin et al., 2006). Excluding 2 basin samples where the extremely low volume filtered caused unreasonably high pSe concentrations, shelf stations also had higher particulate organic

carbon (POC) concentrations than basin stations, with Station 6 having the highest concentration of 12.71 µM POC (data not shown). POC data was generated by Yang Xiang of the Lam Lab at UCSC. Samples were fumed in a desiccator with concentrated HCl to remove carbonate and dried in an oven at 60 ^{o}C overnight before being pelletized in tin discs and measured using a Carbon/Nitrogen Analyzer. The mean pSe:POC of the shelf was 3.6 ± 1.9 x 10^{-6} (Table 3). The shelf pSe:POC ratio was within error of the pSe:POC ratios found in sediment traps in the North Pacific (4.53 x 10^{-6}; Cutter and Bruland, 1984) and suspended matter in the San Francisco Bay (4.2 ± 2.3 x 10^{-6}, n=138, Doblin et al., 2006), but larger than the ratios found in coastal algal blooms (5.97 – 8.20 x 10^{-7}; Wrench and Measures, 1982). The mean C:N ratios of the particulate organic matter (POM) on the shelf, determined by the Lam group at UCSC, was 5.9 ± 1.3 (unpublished results; Table 4), which is within error of the Redfield ratio of 6.6.

Selenium concentrations in shelf sediments was analyzed during this study using archived multi-core and box core samples from the HOTRAX 2005 expedition (Darby et al., 2009). The average total sedimentary Se concentration was 8.2 ± 1.6 nmol Se g^{-1} (n=3; Table 5), which was more than twice the concentration of sediment in Australian Estuary (3.2 nmol Se g^{-1}; Peters et al., 1999) and more than three times the mean concentration of the North San Francisco Bay sediment (2.0 ± 0.7 nmol Se g^{-1}; Doblin et al., 2006). Using the organic carbon concentrations for these cores (Lingle et al., 2007) yielded an average Se:POC ratio of 4.3 ± 1.0 x10^{-5} (Table 5).

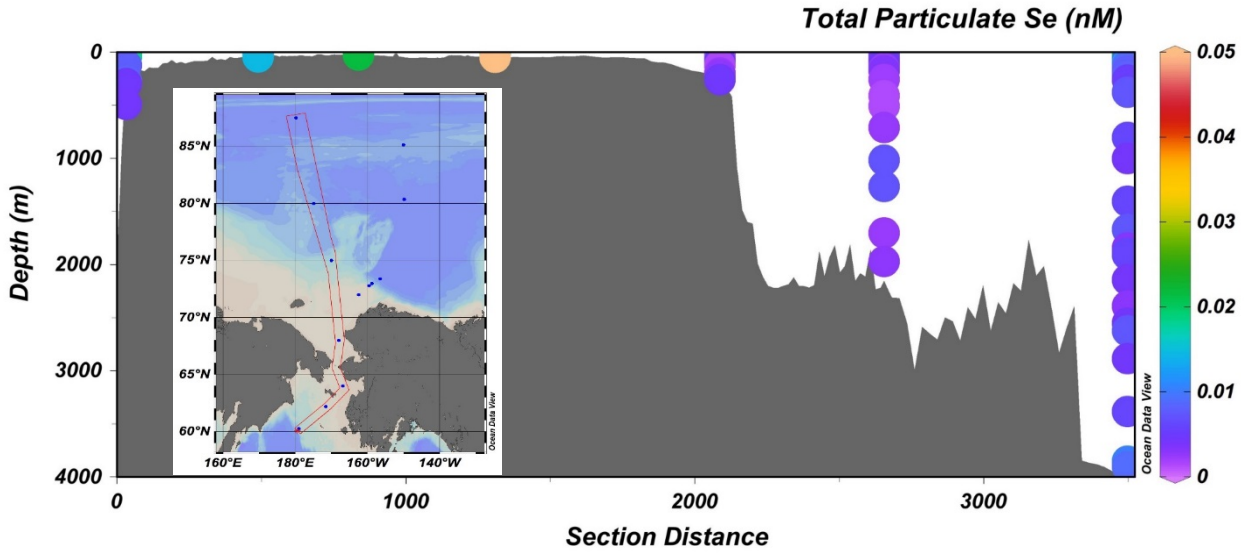

Fig. 13. Particulate Se with depth starting with Station 1 the North Bering Sea on the left and moving through the Makarov Basin northward. Highest pSe concentrations were on the shelf.

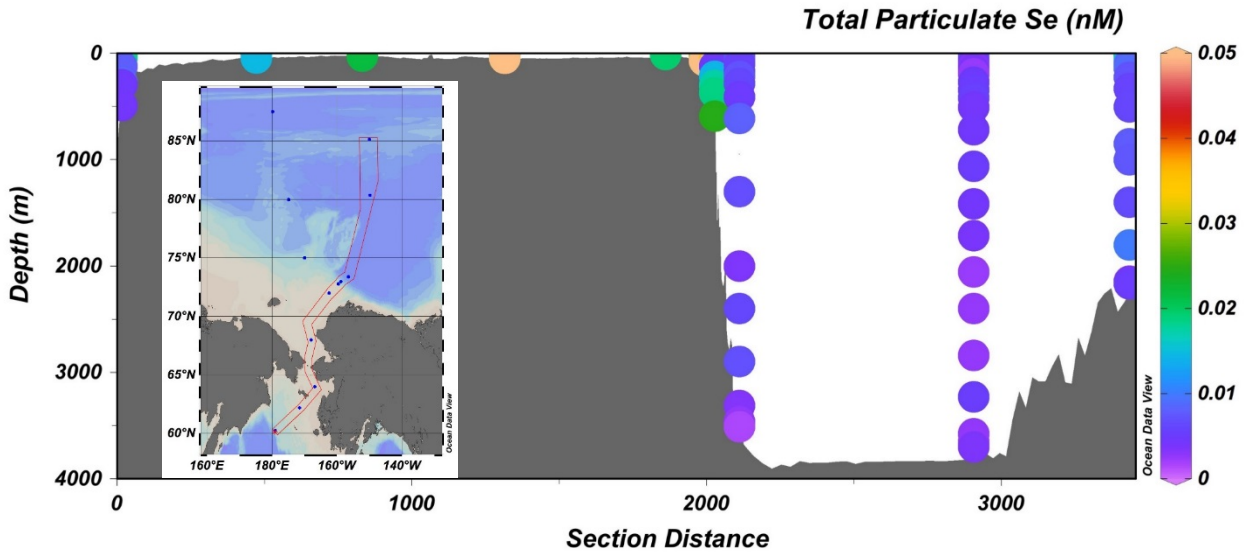

Fig. 14. Particulate Se with depth starting with Station 1 in the North Bering Sea on the left and moving through the Canada Basin northward. Highest pSe concentrations were on the shelf.

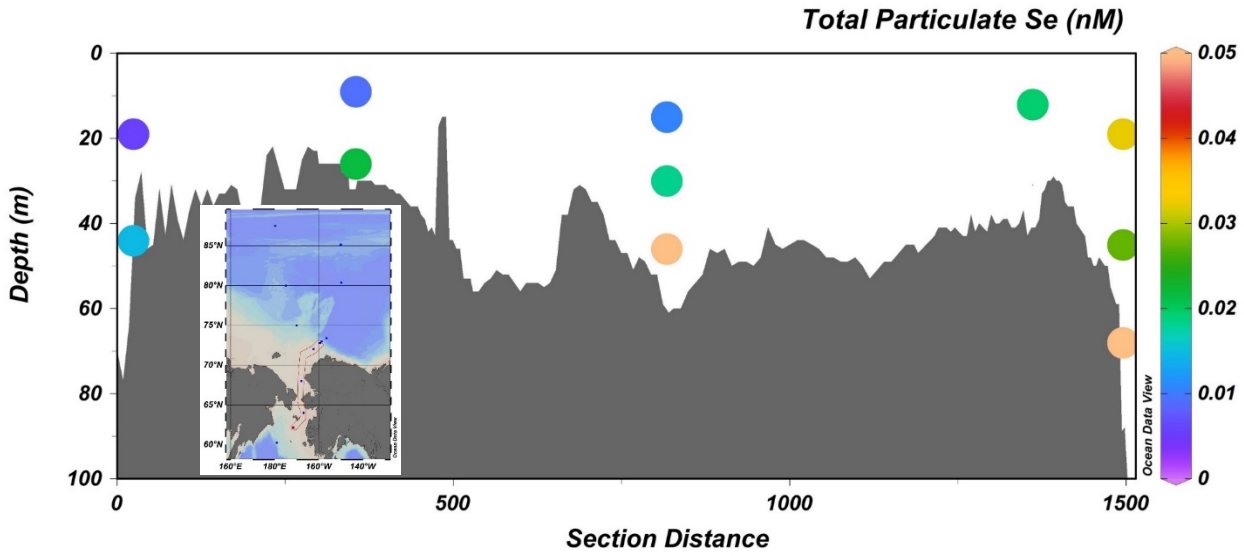

Fig. 15. Particulate selenium with depth on the shelf moving from the south at Station 2 on the left to the north with Station 61 on the right.

Table 3. pSe:POC ratio of the particulate samples from the Arctic Shelf, North Pacific and coastal Atlantic. Error is reported as standard deviation.

	Arctic Shelf	North Pacific [a]	San Francisco Bay [b]	Coastal North Atlantic [c]
pSe:POC (mol:mol)	$3.6 \pm 1.9 \times 10^{-6}$	4.53×10^{-6}	$4.2 \pm 2.3 \times 10^{-6}$	$5.97 - 8.20 \times 10^{-7}$

[a] Cutter and Bruland (1984), [b] Doblin et al. (2006), [c] Wrench and Measures (1982)

Table 4. C:N molar ratios of the shelf Stations determined by the Lam group at UCSC.

Stations	C:N ratio
2	6.7
3	3.9
6	6.9
61	6.7
66	5.9
Average	6.0 ± 1.3

Table 5. Total selenium, and organic carbon concentrations in sediments the Alaskan shelf calculated from cores taken during the 2005 HOTRAX cruise.

	MC-6	MC-8	B4	Mean
Se (nmol g^{-1})	9.3 ± 2.0	8.5 ± 1.6	6.8 ± 0.9	8.2 ± 2.6
Org. C (mmol g^{-1})	0.08	0.01	0.04	0.04
Atomic Se:POC	1.2 ± 0.3 x 10^{-5}	9.5 ± 1.7 x 10^{-5}	2.0 ± 0.2 x 10^{-5}	4.3 ± 1.7 x 10^{-5}

Slope

Station 1 was on the Bering Sea Slope (Fig. 6). Organic selenide, selenite, and total dissolved selenium concentrations increased with depth over the entire sampled water column while selenate concentrations increased with depth to 450 m then decreased to the deepest sample depth of 735 meters, 5 meters from the bottom (Figure 16).

Stations 10 and 60 were on the Chukchi and Alaskan shelf slopes, respectively (Fig. 6). Selenite, selenate, and total dissolved Se showed sub-surface maxima between 100 and 250 m (Figures 17, 18). Organic selenide increased with depth at Station 60 (Fig. 18) and decreased with depth at Station 10 (Fig. 17). Although their profiles are nutrient-like, predicting dissolved selenite and selenate concentrations via application of established relationships with phosphate and silicate in the Pacific (Measures et al., 1980) and Atlantic (Measures and Burton, 1980) underestimated selenite and overestimated selenate concentrations at both slope stations (Figs. 17 and 18). These predictions based on nutrient concentrations will be discussed further in the Basin section to follow.

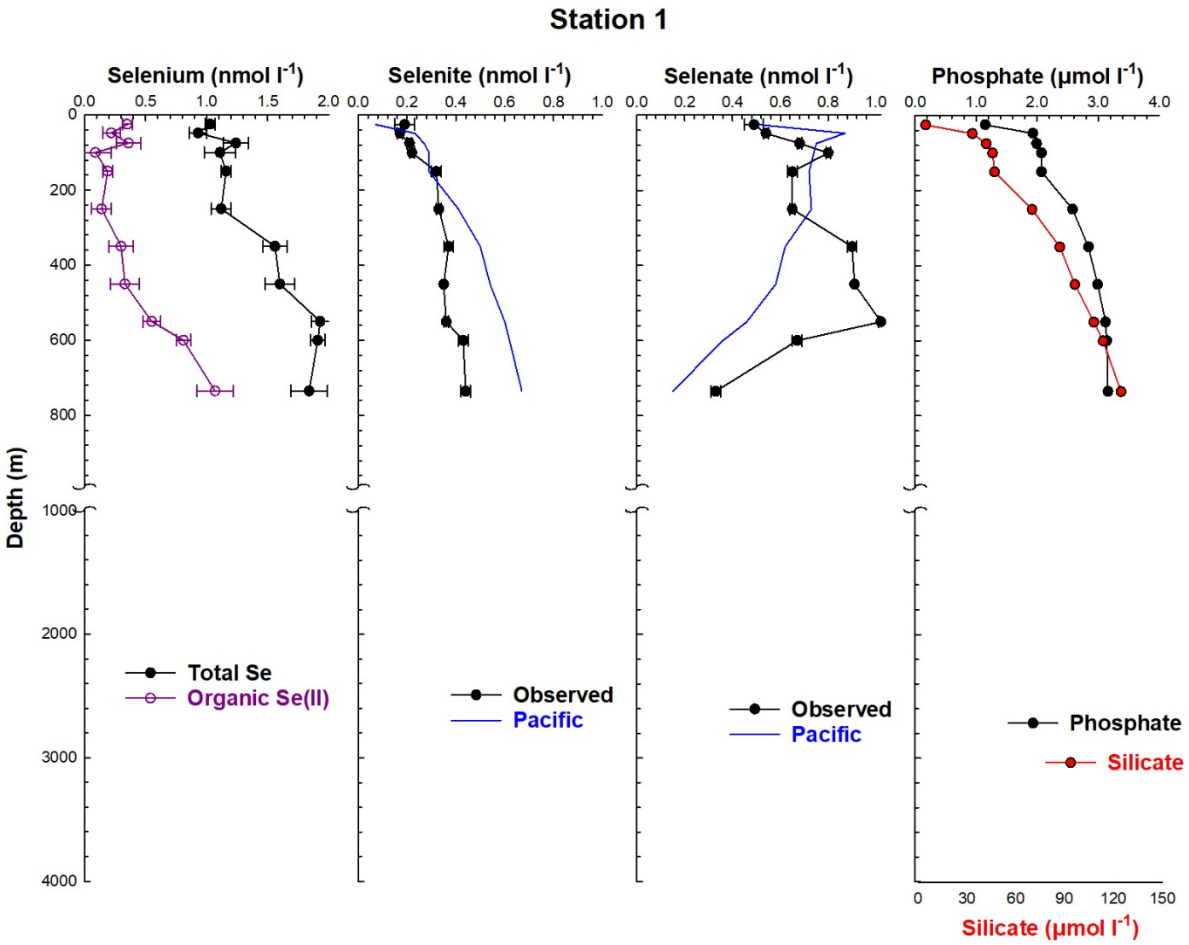

Fig. 16. Depth profiles of organic, selenite, selenate, and total dissolved selenium species, as well as silicate and phosphate at Station 1. The Pacific lines indicate the predicted concentrations using the empirical relationship between the selenium species and silicate and phosphate Measures et al. (1980) found in the Pacific Basin. Error bars as standard deviation for concentrations are shown unless they are smaller than the symbols.

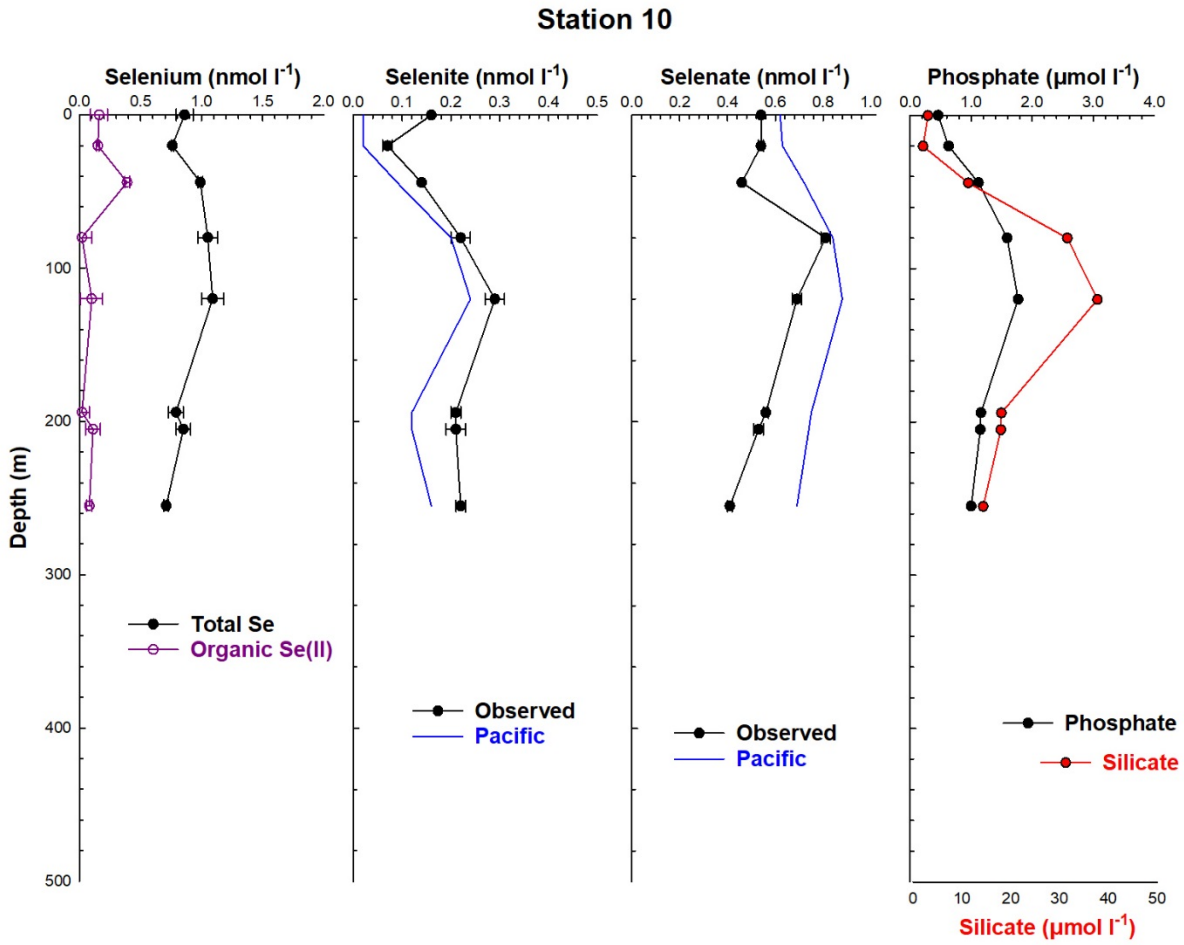

Fig. 17. Depth profiles of organic, selenite, selenate, and total dissolved selenium species, as well as silicate and phosphate at Station 10. The Pacific lines indicate the predicted concentrations using an empirical relationship between the selenium species and silicate and phosphate Measures et al., (1980) found in the Pacific Ocean. Error bars as standard deviation standard deviations for concentrations are shown unless they are smaller than the symbols.

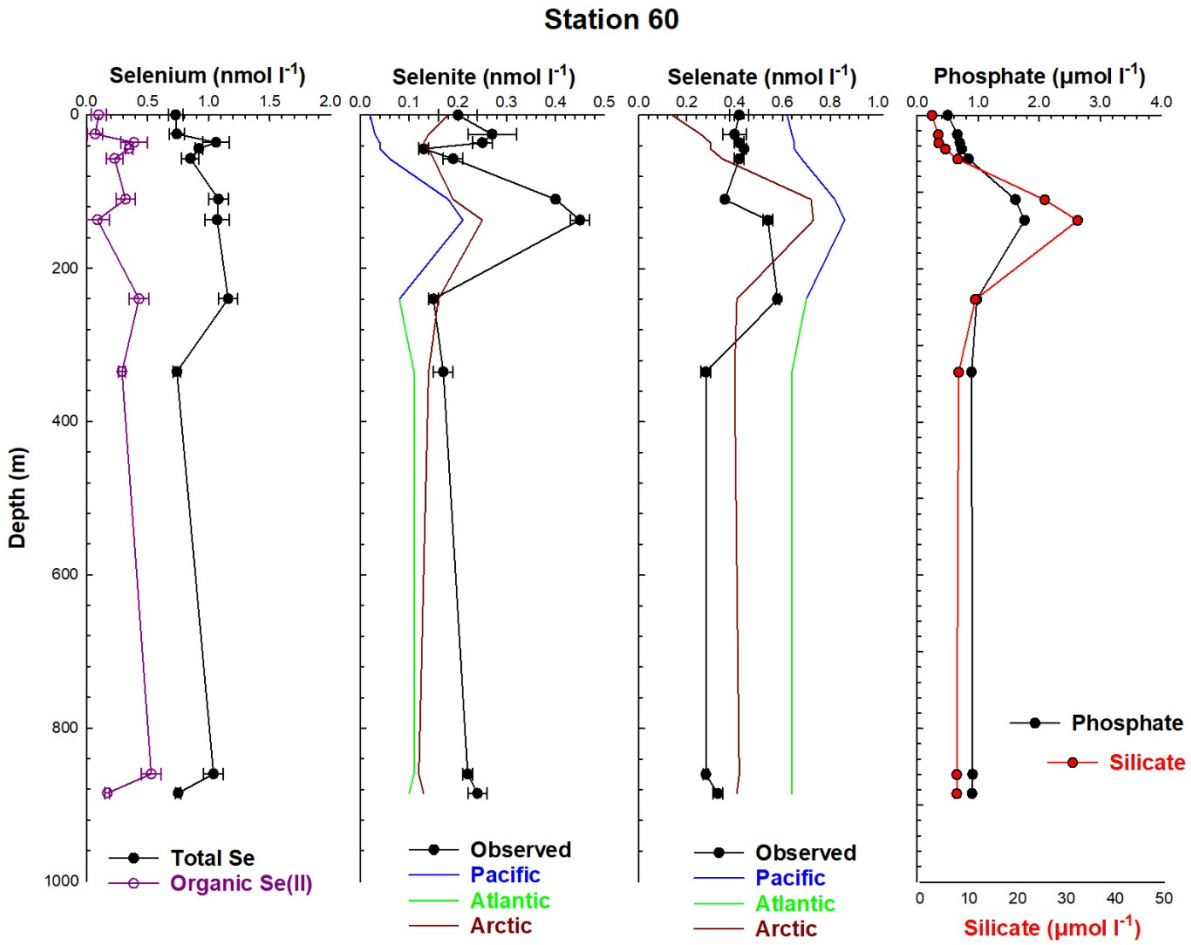

Fig. 18. Depth profiles of organic, selenite, selenate, and total dissolved selenium species, as well as silicate and phosphate at Station 60. The Pacific, and Atlantic lines indicate the predicted concentrations using an empirical relationship between the selenium species and silicate and phosphate found in the Pacific (Measures et al., 1980), and Atlantic (Measures and Burton, 1980) Basins. The Arctic line is the predicted concentration of the selenium species using the empirical relationship between the selenium species and silicate and phosphate in the Amerasian Basin (this study). Error bars are standard deviations for concentrations are shown unless they are smaller than the symbols.

Basin

Stations 19, 43, 48, and 57 were deep water stations inside the Amerasian Basin (Fig. 6). Station 19 was located just north of the Chukchi Shelf in the Makarov Basin. The depth profile of total dissolved selenium (Figure 19) shows a maximum above the cold halocline (Swift et al., 1997; Rudels, 2009) then decreased quickly below the cold halocline, and remained relatively

constant to the bottom. Dissolved selenite increased in concentration to 200 m before dropping and remained relatively constant with depth until increasing in the basin bottom water (greater than 1500 m; Rudels, 2009). Dissolved selenate concentrations were highest at 150 m coinciding with the phosphate and silicate maxima, then decreased to a mid-depth minima at 585 m, then slowly increased with depth (Fig. 19). Dissolved organic selenide was low but present throughout the entire water column with a maximum the near surface.

Station 43 was in the northern Makarov Basin (Fig. 6). Total dissolved selenium concentrations were at a minimum near the surface, then slowly increased with depth (Figure 20). Selenite and selenate showed similar patterns, with near surface minima and gradually increasing with depth. Organic selenide was detectable throughout the water column. Station 48 was in the central Canadian Basin (Fig. 6) and only selenite displayed a nutrient-like profile (Figure 21). Dissolved selenate remained relatively constant with depth and organic selenide was present, but in low concentrations until 3300 m where organic selenide dramatically increased in concentration to the bottom (Fig. 21). Station 57 was in the center of the Beaufort Gyre in the Canada Basin (Fig. 3). Organic selenide made up the majority of the total dissolved Se in the upper 550 m, but below 550 m organic selenide concentrations were low (Figure 22). Selenite and selenate concentrations had surface maxima followed by sub-surface minima to 550m where both species steadily increased with depth.

Selenite and selenate concentrations with depth in the Pacific and Atlantic have been predicted using the relationship between selenium species and silicate and phosphate (Measures et al., 1980; Measures and Burton, 1980). Due to the nutrient like behavior of Se and its typically consistent relationship to silicate and phosphate, an empirical formula for

predicting selenite and selenate concentrations in the North Pacific (Measures et al., 1980) and North Atlantic (Measures and Burton, 1980) has been established by fitting a relationship between the concentrations of selenium species and silicate and phosphate. These established empirical relationships for selenium in Pacific and Atlantic waters were applied to phosphate and silicate concentrations in Arctic waters with Pacific and Atlantic origins, respectively, and plotted alongside observed concentrations in Figs. 19-22. The Pacific fit was applied to waters in the upper 250 meters. Water determined to be mostly Atlantic in origin, deeper than 250 meters, were fitted using the Atlantic equation. The established empirical relationships tended to underestimate selenite and overestimate selenate suggesting that the relationship between selenium species and silicate and phosphate in the Arctic is different than the relationship found in the source water.

An Arctic empirical relationship was generated by fitting selenium species concentration to silicate and phosphate concentrations in order to explore the predictability of Se species concentrations in the Amerasian Basin. Equations of best fit for predicting selenite and selenate concentrations from silicate and phosphate concentrations accounted for, at best, 70% of the variation for selenite at Station 43 (Table 6) and 60% of the selenate variation at Station 19 (Table 7). Applying the best fit equations to the other basin stations resulted in predicted Se species profiles that tended to underestimate selenite and overestimate selenate concentrations, just like the Atlantic and Pacific empirical equations did (Figure 19-22). The inability of phosphate and silicate concentrations to empirically predict selenite or selenate concentrations indicates that other factors are affecting the Se cycle in the Arctic compared to the lower latitude Pacific and Atlantic Oceans.

Table 6. Empirical relationship between selenite and silicate and phosphate generated by fitting silicate and phosphate concentrations to selenite concentrations.

Station	equation	R^2
19	$0.3104 + 0.0172Si – 0.3491PO_4$	0.498
43	$–0.2784 – 0.0157Si + 0.6976PO_4$	0.702
48	$0.3459 + 0.0140Si – 0.3208PO_4$	0.061
57	$0.401 + 0.02001Si – 0.4540PO_4$	0.079

Table 7. Empirical relationship between selenate and silicate and phosphate generated by fitting silicate and phosphate concentrations to selenate concentrations.

Station	equation	R^2
19	$–0.2913 – 0.02071Si + 0.9577PO_4$	0.595
43	$–0.0485 – 0.0134Si + 0.5413PO_4$	0.236
48	$–0.3522 – 0.0510Si + 1.317PO_4$	0.201
57	$0.5592 + 0.0101Si – 0.3919PO_4$	0.069

Suspended particulate Se (pSe) concentrations in the deep basins were extremely low, with the average concentration being 0.06 ±0.04 nM (n=91) (Table 8). Basin POC concentrations, determined by the Lam group at UCSC, averaged 0.22 ± 0.27 μM (n=89; Table 8). The average pSe:POC molar ratio in the deep basins ($2.78 \pm 1.51 \times 10^{-5}$) was 10 times larger than the pSe:POC molar ratio of the shelf Stations ($0.36 \pm 0.79 \times 10^{-5}$).

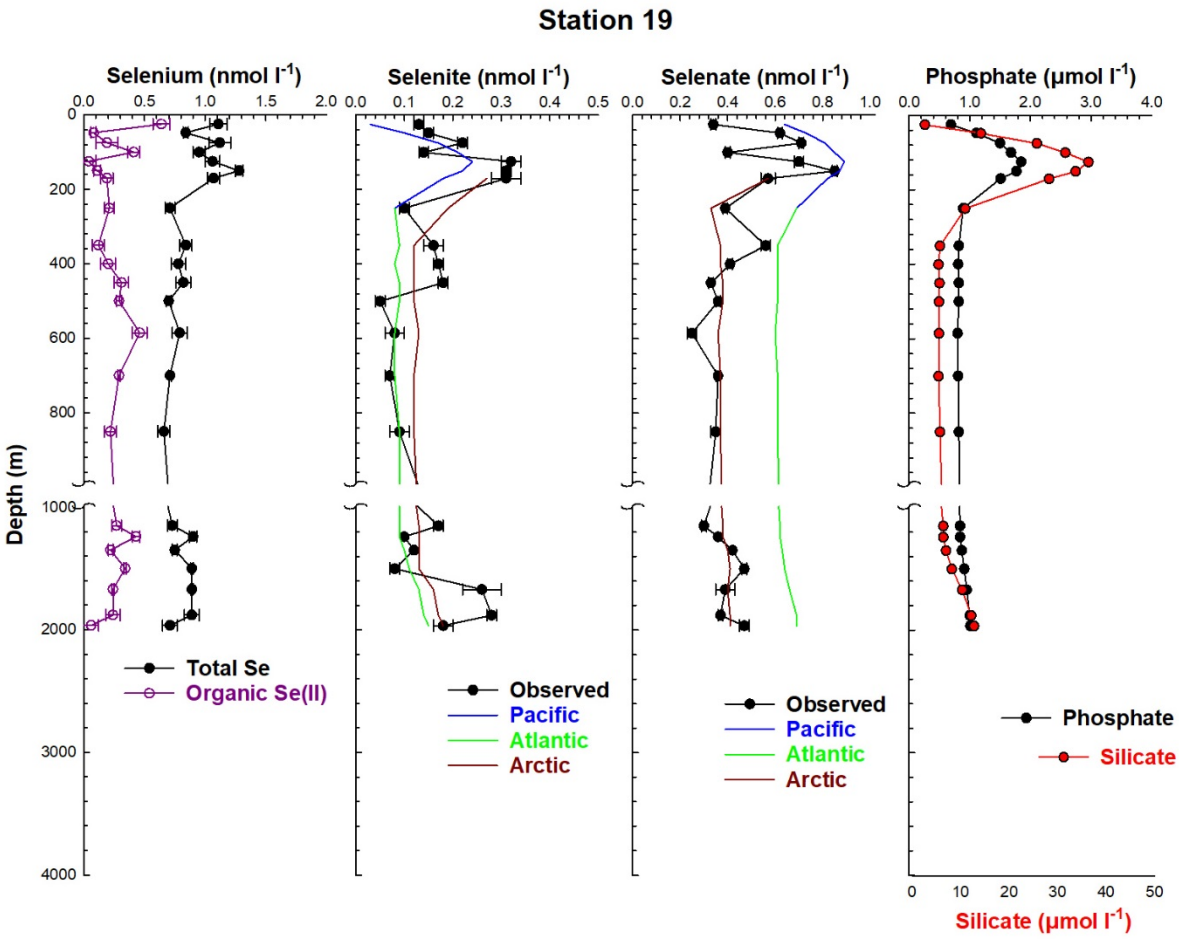

Fig. 19. Depth profile of organic, selenite, selenate, and total dissolved selenium species, as well as phosphate and silicate at Station 19. The Pacific and Atlantic lines indicate the predicted concentrations using an empirical relationship between the selenium species and silicate and phosphate found in the Pacific (Measures et al., 1980), and Atlantic (Measures and Burton, 1980) Basins. The Arctic line is the predicted concentration of the selenium species using the empirical relationship between the selenium species and silicate and phosphate in the Amerasian Basin (this study). Error bars as standard deviations for concentrations are shown unless they are smaller than the symbols.

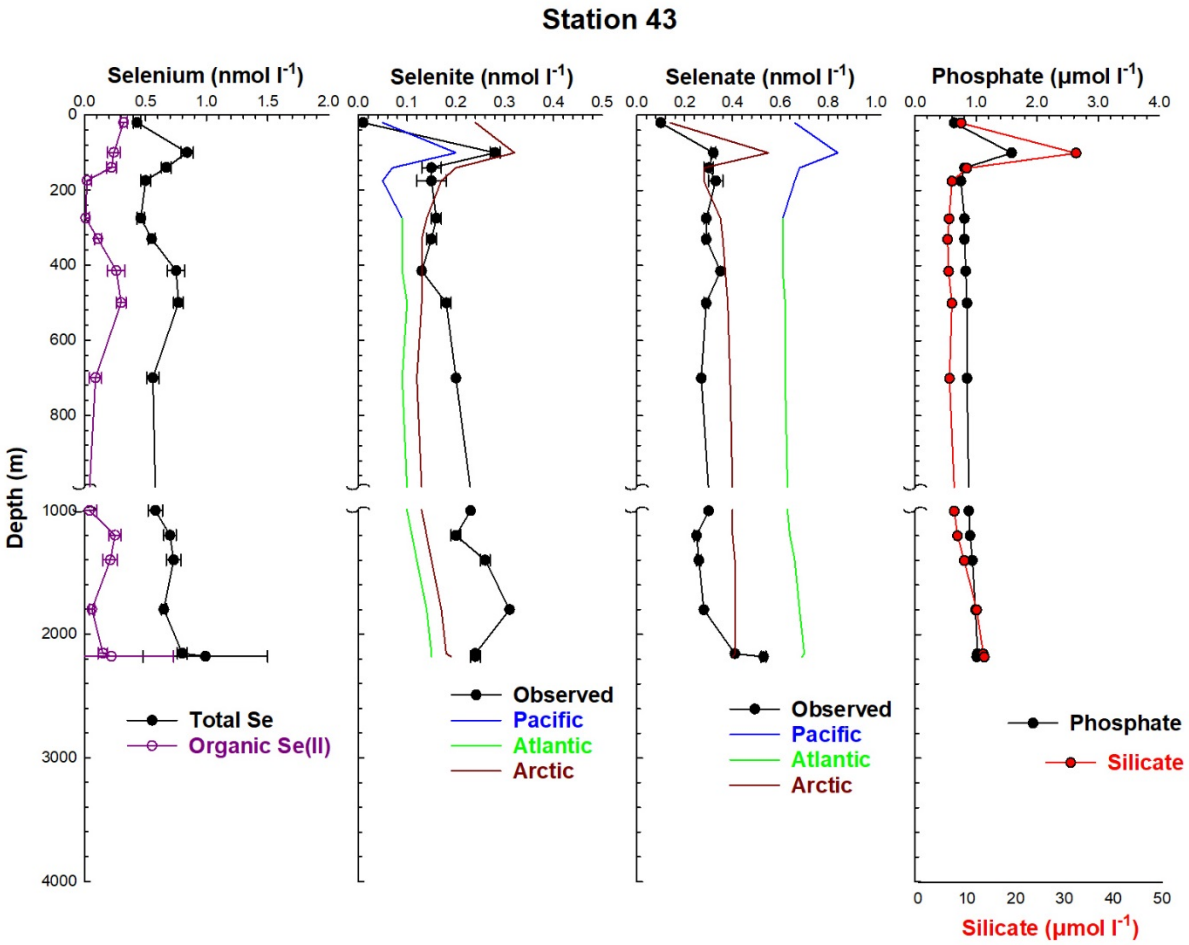

Fig. 20. Depth profile of organic, selenite, selenate, and total dissolved Se as well as phosphate and silicate at Station 43. The Pacific and Atlantic lines indicate the predicted concentrations using an empirical relationship between the selenium species and silicate and phosphate found in the Pacific (Measures et al., 1980), and Atlantic (Measures and Burton, 1980) Basins. The Arctic line is the predicted concentration of the selenium species using the empirical relationship between the selenium species and silicate and phosphate in the Amerasian Basin (this study). Error bars as standard deviations for concentrations are shown unless they are smaller than the symbols.

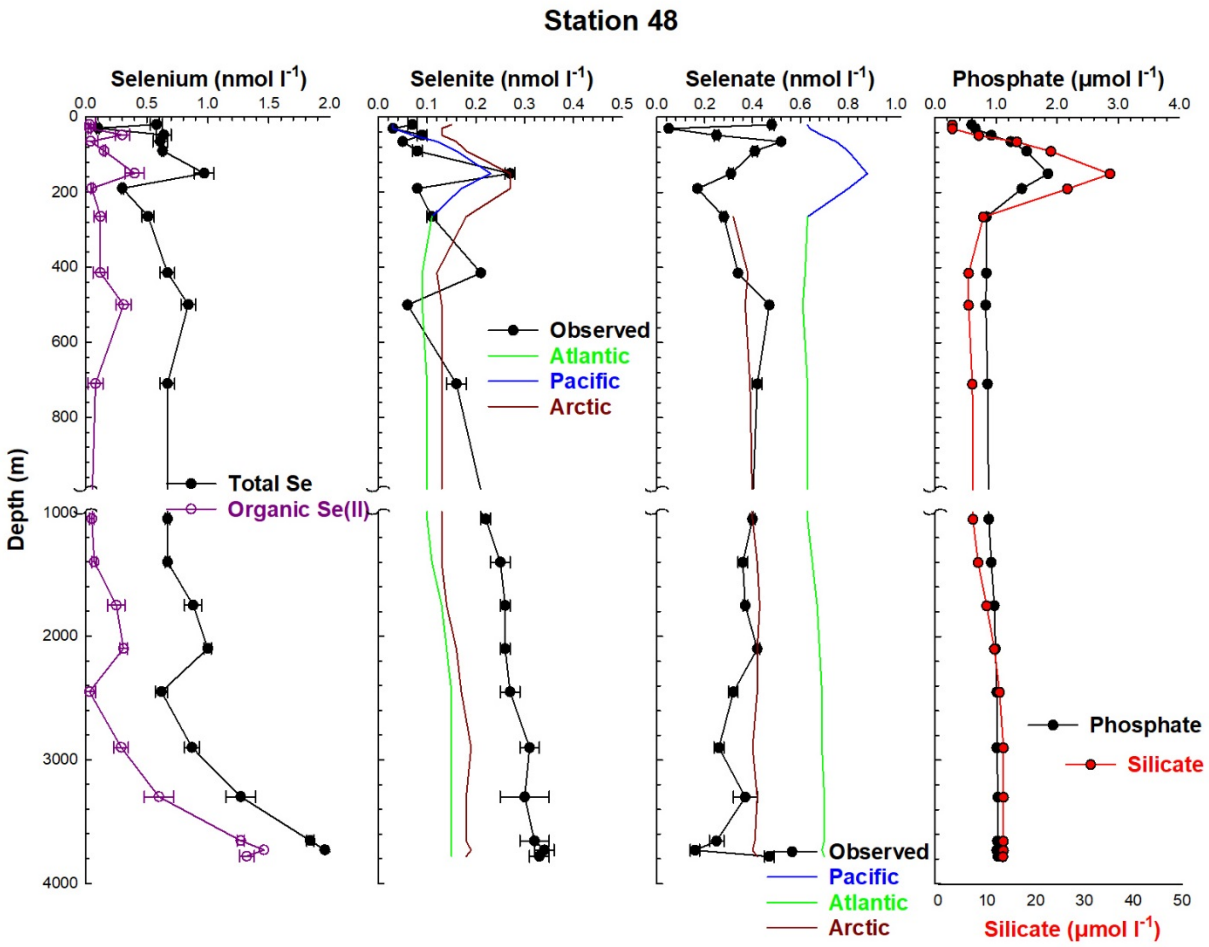

Fig. 21. Depth profile of organic, selenite, selenate, and total dissolved Se as well as phosphate and silicate at Station 48. The Pacific and Atlantic lines indicate the predicted concentrations using an empirical relationship between the selenium species and silicate and phosphate found in the Pacific (Measures et al., 1980), and Atlantic (Measures and Burton, 1980) Basins. The Arctic line is the predicted concentration of the selenium species using the empirical relationship between the selenium species and silicate and phosphate in the Amerasian Basin (this study). Error bars as standard deviations for concentrations are shown unless they are smaller than the symbols.

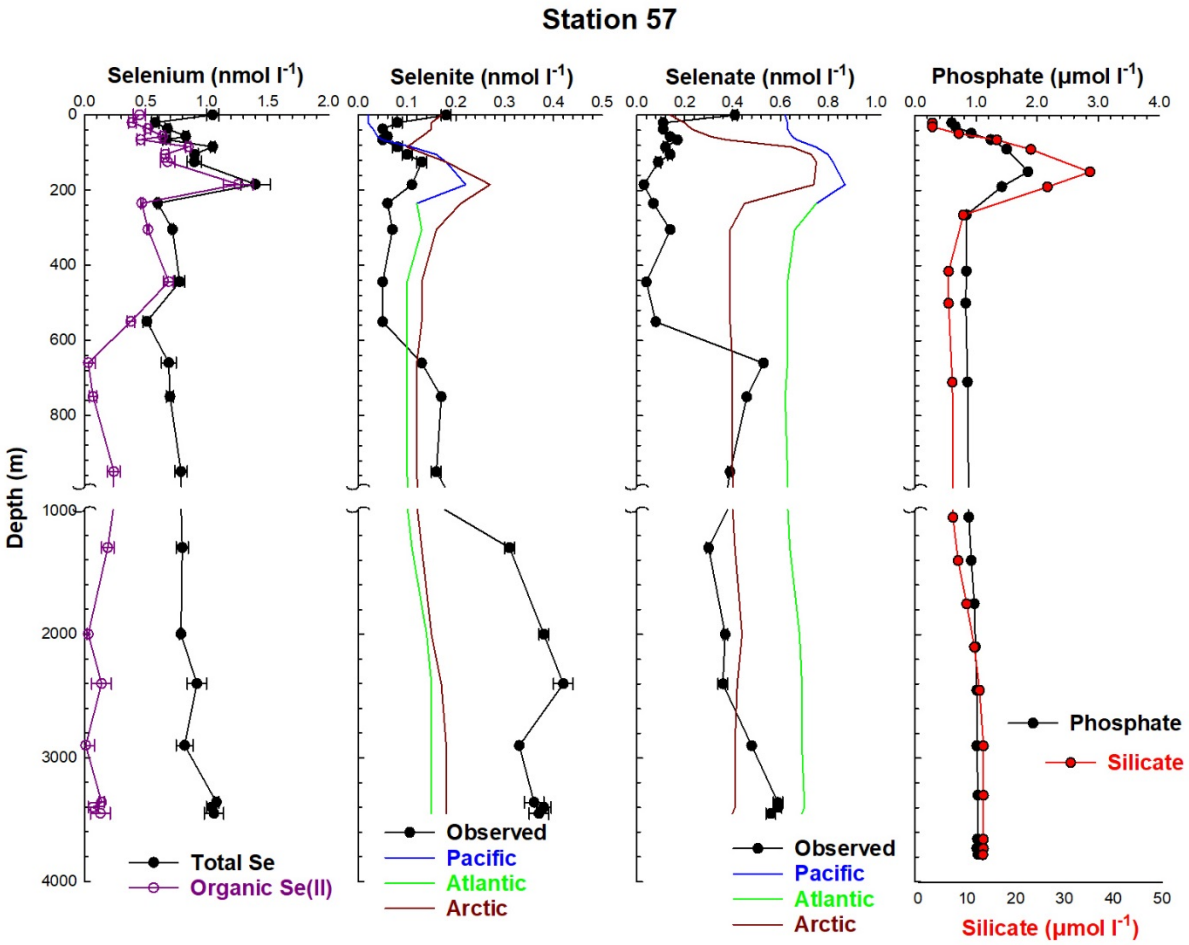

Fig. 22. Depth profile of organic, selenite, selenate, and total dissolved Se as well as phosphate and silicate at Station 57. The Pacific and Atlantic lines indicate the predicted concentrations using an empirical relationship between the selenium species and silicate and phosphate found in the Pacific (Measures et al., 1980), and Atlantic (Measures and Burton, 1980) Basins. The Arctic line is the predicted concentration of the selenium species using the empirical relationship between the selenium species and silicate and phosphate in the Amerasian Basin (this study). Error bars as standard deviations for concentrations are shown unless they are smaller than the symbols.

Table 8. Particulate Se and POC concentrations at the basin stations. n is the number of samples.

	Average pSe (nM)	Standard Deviation (nM)	n	POC (µM)	Standard Deviation (µM)	n	pSe:POC (mol/mol)
Basin Stations	0.006	0.004	91	0.22	0.27	90	$2.8 \pm 1.52 \times 10^{-5}$
Shelf Stations	0.024	0.016	11	6.65	8.33	11	$3.6 \pm 1.9 \times 10^{-6}$

Under ice

Sea ice cover is a unique attribute of the Arctic Ocean when compared to the Pacific, Atlantic, and Indian Oceans. Unfortunately, ice was not analyzed for Se and only 1 under ice Se profile was obtained in the North Makarov Basin. Selenite concentrations were much lower than selenate concentrations, but neither showed a trend with depth (Table 9). Dissolved selenide increased steadily with depth from 0.13 nM one meter below the ice to 0.42 nM at 20 meters, which was slightly less than the total selenium species concentration at 20 m at the nearby ice free station 43 (0.43 ± 0.01 nM), suggesting slight, if any, dilution of Se due to ice melt.

Table 9. Under ice dissolved Se species concentrations in the north Makarov Basin.

Depth (m)	Se(IV) (nM)	Se(VI) (nM)	Se(II) (nM)	Se(T) (nM)
1	0.02	0.32	0.13	0.47
5	0.08	0.19	0.36	0.62
20	0.02	0.25	0.42	0.70

Distribution and crustal enrichment of aerosol selenium

Atmospheric samples were collected throughout the cruise by the Buck group at Skidaway Institute of Oceanography. Aerosol Se concentrations were low throughout the entire cruise (Figure 23), with an average aerosol Se concentration of 7.4 ± 3.5 x 10^{-4} nmol m^{-3} (n=13, Table 10). The Arctic Se aerosol concentrations were lower than previous Arctic and Northern Pacific samples. Maenhaut et al. (1989) determined an average Se concentration in the Norwegian Arctic of 25.3 ± 8.9 x 10^{-4} nmol m^{-3} (n=98). Mosher et al. (1987) saw increasing atmospheric Se concentration with increasing latitude on islands in the North Pacific, with a maximum concentration of 31.7 ± 20.3 x 10^{-4} nmol m^{-3} (n=52, Table 10).

Table 10. Atmospheric Se concentrations and crustal enrichment factors in the Arctic, North Pacific, and North Atlantic

Sample ID	Concentration (x 10^{-4} nmol m^{-3})	Crustal Enrichment Factor
A1	1.6	3703
A2	3.1	4325
A3	2.7	3540
A4	8.3	13457
A6	4.2	1540
A7	7.8	3198
A8	11	5942
A9	8.5	11009
A10	8.3	7131
A11	14	5011
A12	8.7	11420
A13	11	66698
A14	8.4	12867
Arctic GEOTRACES mean	7.4 ± 3.5 (n=13)	11526 ± 17050 (n=13)
Norwegian Arctic [a]	25.3 ± 8.9 (n=98)	
North Pacific (2010) [b]	20 ± 10 (n=46)	3030 ± 2800 (n=46)
North Pacific (1987) [c]	31.7 ± 20.3 (n=52)	
North Atlantic [d]	4.8 ± 3.3 (n=157)	8673 ± 270 (n=132)

[a] Maenhaut et al., (1989), [b] Ranville et al., (2010), [c] Mosher et al. (1987), [d] Arimoto et al., (1992)

Crustal Enrichment factors (EF) were determined by dividing the Se:Al ratio of the sample to the established Se:Al crustal ratio of 5.95 x 10^{-7} (g/g; Taylor and McLennan, 1985). Aluminum concentrations were determined by the Buck Lab. Despite the low Se concentrations, the aerosol samples were highly enriched in Se (Figure 24). The EF of the samples ranged from 1540 – 66698, with an average of 11526 ± 17050 (n=13, Table 10). These Arctic aerosol samples had high EF values like in the North Pacific (3030 ± 2800, range 91 – 13700, n=46; Ranville et al., 2010) and were within the range of EF in North Atlantic aerosol particles (30 – 570,000; Arimoto et al., 1992). These high EF values can only be explained by a gas phase source of Se either from distant anthropogenic fossil fuel combustion or natural volatile Se emissions. These sources will be discussed in the atmospheric flux section to follow.

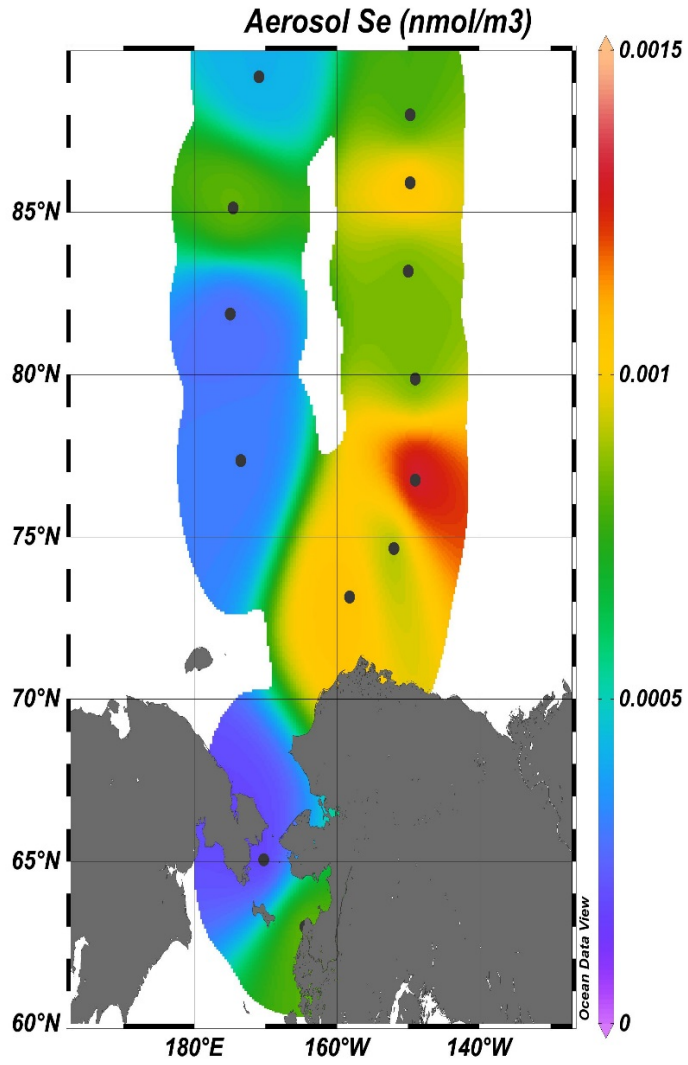

Fig. 23. Aerosol Se concentrations collected during the U.S. Arctic Ocean GEOTRACES GN01 cruise.

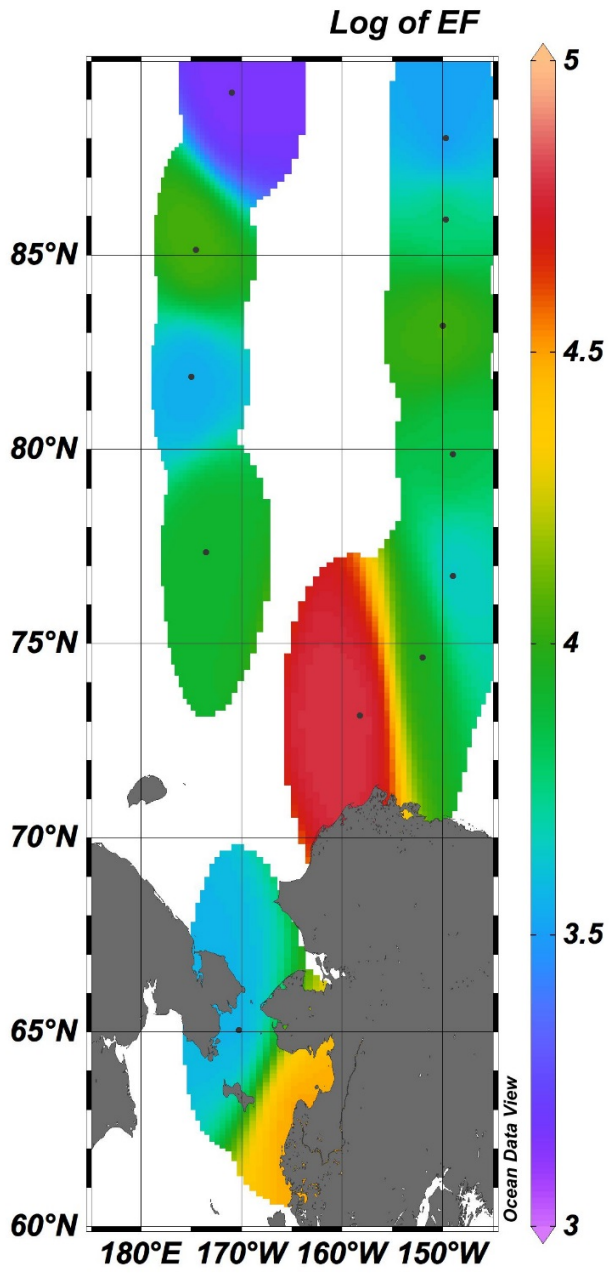

Fig. 24. Log of the crustal enrichment factor of Se aerosols collected during the U.S. Arctic Ocean GEOTRACES GN01 cruise

CHAPTER 4
RATES OF SELENIUM TRANSFER AND TRANSFORMATION IN THE AMERASIAN BASIN

In general, selenium cycling in the Amerasian Basin was roughly similar as that in other oceans, with similar inputs and removals and suspended particle concentration being much less than the dissolved concentration. However, the empirical relationships between dissolved selenium species and silicate and phosphate described in Chapter 3 underestimated selenite and overestimated selenate concentrations unlike in the Atlantic and Pacific Oceans. To help explain the differences, the fluxes and rates that make the Se cycle in the Amerasian Basin unique are quantitatively described zonally, starting with the shelf and slope and moving into the deep water basins.

Shelf and slope

The Pacific Ocean flows into the Arctic Ocean through the Bering Strait. Annual Se input from the Pacific was estimated using the DIA Se concentration of the Bering Strait (Station 4; 1.1 ± 0.1 nM; n=4; Table 2) and the annual net northward flow of 1.0 ± 0.1 Sv through the Bering Strait (Woodgate, 2017). In this way, the net annual Pacific input of Se was estimated to be $3.3 \pm 0.2 \times 10^{7}$ mol Se yr^{-1} (Table 11).

The Arctic Ocean receives a disproportionally large amount of riverine discharge for the relatively small size of its basin (Carmack et al., 2016). Despite the large influx of riverine water, there are currently no selenium data for Arctic rivers.

Table 11. Input, internal cycling, and removal fluxes of selenium in the Amerasian Basin.

Flux Type	Se Flux	Magnitude (mol Se yr^{-1})
Input	Atmospheric Deposition	$2.5 \pm 1.3 \times 10^{6}$
Input	Atlantic to Amerasian Basin Flow	$6.9 \pm 0.5 \times 10^{7}$
Input	Pacific to Amerasian Basin	$3.3 \pm 0.2 \times 10^{7}$
Input	Riverine to Amerasian Basin	$2.0 \pm 1.5 \times 10^{6}$
Internal Cycling	Shelf Biological Uptake	$7.9 \pm 0.4 \times 10^{7}$
Internal Cycling	Basin Biological Uptake	$7.7 \pm 0.9 \times 10^{7}$
Removal	Amerasian Shelf Sedimentation	$8.7 \pm 1.4 \times 10^{6}$
Removal	Deep Amerasian Basin Sedimentation	$4.5 \pm 0.7 \times 10^{5}$
Removal	Amerasian Basin Sedimentation	$9.2 \pm 1.4\ 10^{6}$
Removal	Amerasian Basin to Canadian archipelago	$7.1 \pm 0.5 \times 10^{7}$
Removal	Amerasian Basin to Fram Strait	$2.1 \pm 0.1 \times 10^{7}$
Input	Total Input	$1.0 \pm 0.5 \times 10^{8}$
Removal	Total Removal	$1.0 \pm 0.1 \times 10^{8}$

A riverine input of dissolved Se was estimated using the world river average concentration of total dissolved Se (1.82 ± 1.46 nM, n=28; Cutter, 1989b) and the total annual discharge of the rivers that empty into the Amerasian Basin (1115.96 $km^3\ yr^{-1}$; Holmes et al., 2015). Multiplying the discharge volume by the average Se riverine concentration resulted in a riverine input of $2.0 \pm 1.5 \times 10^{6}$ mol Se yr^{-1} (Table 11). This calculated input of dissolved Se using the world river average is an order of magnitude lower than the input from the Pacific Ocean (Table 11), but does not diminish its importance to coastal regions near the discharges and adjacent basins.

The dissolved Se entering the euphotic zone of the Amerasian Shelf is available for incorporation by phytoplankton. Biological uptake of Se was estimated using the annualized

primary production of the Chukchi Sea (90 g C m^{-2} yr^{-1}) established by Hill and Cota (2005), the area of the Amerasian Shelf, and the pSe:C ratio of 3.6 ± 1.9 x 10^{-6} (Table 8) found on the shelf where most of the highly seasonal primary productivity occurs in the Arctic (Hill and Cota, 2005; Sakshaug, 2004). The Amerasian Shelf area was calculated by multiplying the area of the Amerasian Basin (8.43 x 10^6 km^2; Codispoti et al., 2013), to the shelf to basin ratio (0.35; Kadko and Muench, 2005). An annual biological uptake of 7.9 ± 0.4 x 10^7 mol Se was calculated for the Amerasian Shelf (Table 11). Biological uptake is the first step in the highly active biological pump of the Amerasian Basin (Hill et al., 2013) that results in the removal of Se from the upper water column.

The Amerasian shelf sedimentation flux of Se was calculated by multiplying the mean surface sediment Se concentration (8.2 ± 2.6 nmol g^{-1}; Table 5) by the sedimentation rates on the shelf. The surface sediment Se concentration as well as a sedimentation rate were determined from cores taken on the Alaskan Shelf during the 2005 HOTRAX expeditions (Darby et al., 2009). Shelf sedimentation rates reported in the literature differ throughout the Arctic, ranging from 1 x 10^{-3} cm yr^{-1} (Andrews and Dunhill, 2004) to 1.1 cm yr^{-1} (Darby et al. 2009). This study used sediments from boxcore and multicore samples taken during the 2005 HOTRAX expedition to generate a shelf sediment concentration; therefore, the sedimentation rate associated with those specific cores was used (0.04 cm yr^{-1}; Darby et al. 2009). The sedimentation rate was converted into a depositional flux using the equation (Berner, 1980):

$$R = \rho_s * w * (1\text{-porosity}) \quad (3)$$

Where ρ_s = the density of the sediment (2.65 g cm^{-3}; Darby et al., 2009), w = sedimentation rate (0.04 cm yr^{-1}; Darby et al., 2009) and the porosity of soft, slightly organic clay (0.66; Terzaghi et

al., 1996) was used. The flux calculated from the cores (0.30 ± 0.05 nmol cm^{-2} yr^{-1}) was extrapolated to the entire Amerasian shelf by multiplying this sedimentation rate by the surface area of the Amerasian shelf (4.92 x 10^6 km^2), resulting in a sedimentation flux of 8.7 ± 1.4 x 10^6 mols Se yr^{-1} (Table 11). The sedimentation flux is an order of magnitude less than the biological uptake of Se (Table 11), suggesting strong regeneration and recycling of selenium in the water column.

Basins

Shelf fluxes, like deposition into, and diffusion out of the sediment, as well as shelf redox processes can greatly alter selenium concentration and speciation, causing the water entering the basin to have a different Se composition than the water that entered the shelves. ^{228}Ra in an offshore basin has a shelf sediment source that can be quantified using activities and half life. The flux of an element from the shelf can then be generated using its ratio to ^{228}Ra and the Ra flux (Charette et al., 2016):

$$\text{Se flux} = {}^{228}\text{Ra flux} * (\Delta\text{Se}/\Delta{}^{228}\text{Ra}) \quad (4)$$

This method requires a linear relationship between Se and ^{228}Ra concentrations. The linear regression between total dissolved selenium and ^{228}Ra concentrations had an r^2 of 0.001 (Figure 25) indicating that there was no significant relationship between Se and ^{228}Ra and therefore the shelf was not a significant source or sink of selenium to the Amerasian Basin.

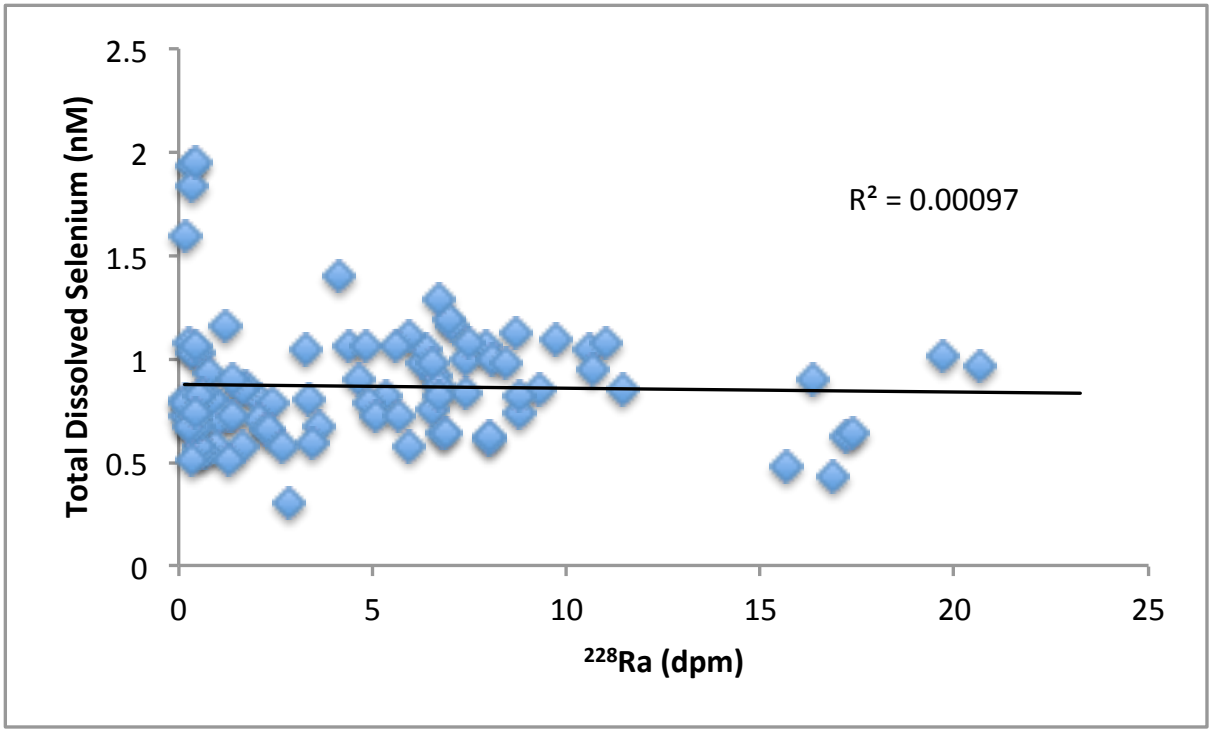

Fig. 25. Relationship between ^{228}Ra and total dissolved selenium in the upper 500 meters of the Amerasian Basin.

Primary productivity in the Arctic Ocean mainly occurs on the shelves (Hill et al., 2013), but some productivity does occur in the basins. Fernandez-Mendez et al., (2015) reported that Arctic Basin algae produce 2.8 ± 0.6 x 10^{12} mol C yr^{-1}. Multiplying this production rate by the observed basin pSe:POC ratio 2.8 ± 1.5 x 10^{-5} (Table 8) results in a selenium removal rate of 7.7 ± 0.9 x 10^{7} mol Se yr^{-1} (Table 11). This basin biological removal of Se is within error of the calculated biological uptake of Se on the shelf due to the higher pSe:POC ratio in the basin and the larger surface area of the Basin. The shelf is more productive per area, but the basin is larger and had phytoplankton with a higher selenium content, relative to organic carbon. The loss of particulate Se can be calculated using the ^{234}Th flux and observed pSe/^{234}Th ratios. However, ^{234}Th data indicated that there was no measurable particle flux in the basin;

therefore, there was no detectable export of surface produced Se to the deep water (Black, 2018). This lack of a measurable particulate Se flux will be discussed further below.

The Atlantic Ocean is the dominant source of subsurface water in the Amerasian Basin (Aagaard et al., 1981; Aagaard et al., 1985; Swift et al., 1987; Woodgate et al., 2001). Most of the intermediate and all of the deep water in the Amerasian Basin is Atlantic in origin, with the Pacific influence reaching a maximum depth of 500 meters (Swift et al., 1997; Woodgate et al., 2001; Rudels, 2009). Atlantic water entering the Amerasian Basin passes through the Barents Sea and the Kara Sea as a boundary current inflow remaining close to the shelf, but a portion of the inflow enters the Amerasian Basin by crossing over the Lomonosov Ridge as far north as 86.5^{o} N (Woodgate et al., 2001). The Se influx via this Eurasian Basin to Amerasian Basin exchange was estimated using the annual current flow across the Lomonosov Ridge of 3.0 ± 1.0 Sv, which crosses between 500 and 2500 m (Woodgate et al., 2001). This flow was multiplied by the DIA Se concentration found at that depth range for Station 30, the closest sampling Station (~800 km away) to the northernmost inflow, resulting in an influx of $6.9 \pm 0.5 \times 10^{7}$ mol Se yr^{-1} (Table 11).

The Atlantic Ocean is not only a source, but also a major sink for Amerasian Basin Se. Arctic water and dissolved Se moves from the Arctic Ocean to the Atlantic Ocean through the Fram Strait and Canadian Archipelago (CA). There are a few major channels in the CA that Arctic water passes through, with about 45% through the Nares Strait, 15% through the Cardigan Strait, and 40% through Lancaster Sound (http://asof.awi.de/science/projects/4-canadian-arctic-through-flow-cat-study/). Direct current measurements of the Nares Strait were collected and analyzed by Munchow and Melling (2015), and Se flux out of the Nares

Strait was calculated and extrapolated to the entire CA using the aforementioned percentage of flow. A DIA Se concentrations for the flow through the CA and Fram Strait were calculated using proportions of 3 different water masses, the Polar Mixed layer (PML), the cold halocline layer, and the intermediate/Atlantic layer (Rudels 2009), from 5 different sampling stations in the Canada Basin (Table 12). The depth and direction of flow of the different water masses described by Rudels et al.(1994), Jones et al. (1995), Rudels et al. (2004), and ultimately defined by Rudels (2009) are shown in Figs. 3 – 5. PML water had a salinity greater than 30, but less than 32.5 ($30 < S < 32.50$). The Cold Halocline layer was defined as having a potential temperature $\approx 0\ ^{o}C$, and salinity of $32 < S < 34.50$ (Rudels, 2009). Intermediate/Atlantic layer water had a potential temperature of less than $-0.5\ ^{o}C$, and a salinity of $34.50 < S < 34.92$ (Rudels, 2009). The water masses and the percentage of influence each station had on a water mass exiting the western basin was based on the flow direction and the proximity to the designated exit. The CA is shallow, less than 400 m deep (Munchow and Melling, 2015), only allowing the PML and halocline water masses to pass through it. The main PML outflow of the CA flows through Station 30 with some outflow coming from Station 60 (Fig. 3). The circulation of the halocline layer only passes through Station 43 before exiting through the CA. The concentration of the entire water column exiting through the Nares Strait was estimated using a weighted average of the PML and the halocline layer (Table 13). According to salinity and temperature profiles (Munchow and Melling, 2015), the PML accounted for $1/6^{th}$ and the halocline accounted for $5/6^{th}$ of the total water passing through Nares Strait (Table 13), resulting in a weighted DIA concentration of 1.0 nM (Table 14). Removal of dissolved Se through the CA was then estimated by multiplying the flow (1.00 ± 0.08 Sv; Munchow and

Melling, 2015) by the DIA concentration, and then dividing by the percent of total flow through the Canadian Archipelago accounted for by the Nares Strait (45%; Canadian Arctic Throughflow). The calculated net removal flux of Se through the CA was determined to be 7.1 ± 0.5 x 10^7 mol Se yr^{-1} (Table 11).

Table 12. Depth integrated average total Se concentrations (nM) for the different water masses involved in the outflow through the Canadian Archipelago and Fram Strait. N/A = not applicable, indicates that the flow of that water mass at that Station does not leave the basin via the Canadian Archipelago or the Fram Strait.

Station	Polar Mixed Layer (nM)	Halocline (nM)	Intermediate Layer (nM)
30	0.61	0.65	0.68
43	0.43	0.75	0.64
48	N/A	0.60	0.68
57	N/A	1.08	0.73
60	0.84	N/A	N/A

Table 13. Calculations of Se outflow through the Canadian Archipelago. Concentrations are reported as nM. N/A = not applicable.

	Station 30	Station 57	Station 60	Total	Nares Strait
Polar Mixed Layer	0.52 ± 0.10	N/A	0.13 ± 0.02	0.66 ± 0.1	0.11 ± 0.02
Halocline Layer	N/A	1.08 ± 0.40	N/A	1.08 ± 0.40	0.90 ± 0.24

Table 14: Calculations for Se flux through the Canadian Archipelago continued.

Nares Strait Out Flow	1.0 ± 0.2 nM
Nares Strait Volume flux	1.0 ± 0.1 Sv
Nares Strait Annual Se flux	3.2 ± 0.2 x 10^7 mol yr^{-1}
Canadian Archipelago Se Flux	7.1 ± 0.5 x 10^7 mol yr^{-1}

In addition to the outflow of water through the Canadian Archipelago, there is an annual net flow out of the Arctic Ocean through the Fram Strait, with a proportion of the outflow water coming from the Amerasian Basin. Removal of Amerasian Basin dissolved Se through the

Fram Strait was estimated by breaking down the flow into water masses, determining the stations in which the water masses pass through on the way out of the Amerasian Basin, and estimating the proportion of each station in the concentration of the water mass that passes through the Fram Strait. The upper, halocline, and intermediate layers of the Amerasian Basin exit through the Fram Strait (Rudels, 2012). Distance from the Fram Strait varied for each station depending on the flow path of the water layer, but Station 30 was always the closest station to the Fram Strait and thus received the highest weighted average when estimating the selenium concentration exiting through the Fram Strait (Table 15). The PML water mass passed through Station 43 and Station 30 shortly before exiting through the Fram Strait (Fig. 3). Station 30 was much closer to the Fram Strait via the flow path of the PML water mass (Fig. 3); therefore, the PML at Station 30 was estimated to reflect 95% of the Se concentration in the PML water mass in the Fram Strait with Station 43 representing 5% (Table 15). The halocline layer passed through Stations 43, 48, 57, and 30 before exiting through the Fram Strait (Fig. 4). Station 43 was furthest from the Fram Strait via the halocline water circulation path, then Stations 48, and 57, with Station 30 being the closest (Fig. 4); therefore, Stations 43, 48, 57, and 30 were given a weighted average of 5%, 10%, 15%, and 70% respectively (Table 15). The intermediate layer moves through Stations 48, 57, 43, and 30 before exiting the basin, with Station 48 being the furthest and Station 30 being the closest (Fig. 5). Weighted averages were done according to distance with stations 48, 57, 43, and 30 receiving 10%, 15%, 30%, and 45% respectively (Table 15). Weight averaging the concentrations of the layers at the different stations resulted in Se concentrations of the Amerasian Basin water masses that exit through the Fram Strait (Table 16). The depth of the Fram Strait is about 2500 m deep (Schauer, et al.,

2004; Marnela et al., 2016), and the temperature and salinity profiles of the Strait (Marnela et al., 2016) dictated that the upper, halocline, and intermediate layers were 50, 250, and 2200 m thick, respectively. The Amerasian Basin was estimated to make up a maximum of 50% of the Arctic Ocean outflow through the Fram Strait (Marnela et al., 2016). Multiplying the weighted DIA Se concentration by the net annual southern flow of the Fram Strait (2.0 ± 0.5 Sv; Rudels et al., 2009) resulted in an estimation of 2.2 ± 0.8 x 10^7 mol Se exiting the Amerasian Basin through the Fram Strait per year (Table 11).

Table 15. Weighted percent of the stations to the final selenium concentration of the Amerasian Basin water masses that exit through the Fram Strait. N/A indicates that the water mass does not pass through that station before exiting the Fram Strait.

Station	Polar Mixed Layer	Halocline Layer	Intermediate Layer
Station 30	95%	70%	45%
Station 43	5%	5%	30%
Station 48	N/A	10%	10%
Station 57	N/A	15%	15%

Table 16. Calculations of Amerasian Basin Se outflow through the Fram Strait. The concentrations contributed by each station have been weighted based on the distance from the Fram Strait to the station via the flow path of the water mass. N/A indicates that the water mass did not pass through that station before exiting the Fram Strait. Concentrations are reported as nM.

Water Mass	Station 30	Station 43	Station 48	Station 57	Total
Polar Mixed Layer	0.58 ± 0.12	0.02 ± 0.001	N/A	N/A	0.60 ± 0.02
Halocline	0.46 ± 0.04	0.02 ± 0.003	0.06 ± 0.04	0.19 ± 0.07	0.73 ± 0.09
Intermediate Layer	0.31 ± 0.06	0.19 ± 0.03	0.07 ± 0.03	0.12 ± 0.01	0.68 ± 0.07

Selenium in the Amerasian Basin is also removed from the water column via sedimentation. Selenium sedimentation flux in the deep basin was estimated using the total Se concentration of the shelf cores (Table 5), the area of the deep basin (5.48 x 10^6 km^2) calculated from 65% (Kadko and Muench, 2005) of the total Amerasian Basin area (8.43 x 10^6 km^2;

Codispoti et al., 2013), and a Canada Abyssal Plain pelagic sedimentation rate of 10 mm per 1000 years established by Grantz et al. (1996). This sedimentation rate ignores episodic turbidite deposits because the selenium in turbidites has already been removed from the water column. The basin sedimentation flux was estimated to be $4.5 \pm 0.7 \times 10^5$ mol yr^{-1} (Table 11). This sedimentation rate assumes that the apparent lack of particle flux determined by the ^{234}Th data was either temporary or below the method's detection limit. The deep basin sedimentation rate was an order of magnitude lower than the sedimentation rate on the shelf (Table 11), which is consistent with the low particulate Se concentrations (Figs. 13-14). The deep basin sedimentation flux was more than two orders of magnitude lower than the basin biological uptake ($7.7 \pm 0.9 \times 10^7$ mol yr^{-1}; Table 11), suggesting that most of the particulate Se was regenerated in the upper water column. Biological uptake of Se was roughly the same in the basin and shelves ($7.7 \pm 0.9 \times 10^7$ and $7.9 \pm 0.4 \times 10^7$, respectively; Table 11). The difference likely occurred due to higher Se:C phytoplankton (Table 4) and larger surface area in the deep basin. The lack of particulate Se or organic matter in the basin (Figs. 13-14; Table 8) indicates that the regeneration of Se occurs quickly, preventing the accumulation of particulate matter, but regeneration is likely equally as fast on the shelves to prevent accumulation there as well (Figs 13-14; Table 8). Determination of the Se concentration in deep basin sediment would improve the accuracy of this estimate by removing the assumption that the shelf sediment Se concentrations were representative of basin sediment concentrations.

Ice flux out of the Basin is a unique part of the Arctic Ocean water budget. An annual average of 800,000 km^2 of ice export from the Arctic Ocean representing an annual removal of

10% of the sea ice in the Arctic Ocean. (Smedsrud et al., 2013). Unfortunately, there was no selenium data for ice samples, so a selenium removal flux via ice export could not be estimated.

Atmospheric flux

In order to calculate atmospheric deposition of Se to the Arctic Ocean, the aerosol concentrations must be converted to an aerosol deposition rate. A bulk atmospheric deposition velocity was calculated by the Kadko lab at Florida International University using ^{7}Be data collected on the cruise (Kadko et al., 2015). The calculated velocity included both wet and dry deposition and was determined to be 1140 ± 671 m d^{-1}. Combining the aerosol Se concentrations with this deposition rate generated an average atmospheric Se flux of 0.30 ± 0.16 mol km^{-2} yr^{-1}, with a range of 0.07 – 0.57mol km^{-2} yr^{-1} (n=13; Table 11). Extrapolating the average flux across the entire basin using the surface area of the basin (8.43 x 10^{6} km^{2}; Codispoti et al. 2013) resulted in a depositional flux of 2.5 ± 1.3 x 10^{6} mol yr^{-1} (Table 11). The per km^{-2} Arctic depositional rate (0.30 ± 0.16 mol Se km^{-2} yr^{-1}; Table 11) was within the range of the world average atmospheric Se deposition rate (Mosher and Duce, 1987; Table 17), but lower than the Se atmospheric deposition rate in the Equatorial Atlantic (Table 17). For ease of calculations, atmospheric input of Se was assumed to have no ice buffer and entered directly into the surface water, likely overestimating the impact of atmospheric deposition of Se. Despite a potential overestimation of aerosol Se input to surface waters of the Amerasian Basin, Se aerosols deposition was ~10% and ~15% of the selenium input via the Pacific and Atlantic Oceans, respectively (Table 11). Selenium atmospheric deposition is a major source for surface selenium in the Equatorial (Cutter and Cutter, 2001) and North Atlantic Ocean (Cutter

and Cutter, 1998), a characteristic not seen in the Amerasian Basin, with inputs from the Atlantic and Pacific Oceans being the dominant sources.

Table 17. Atmospheric deposition of Se in the Amerasian Basin, Equatorial Atlantic and world average.

Location	Deposition rate
Amerasian Basin (total basin) [a]	$2.5 \pm 1.3 \times 10^6$ mol Se yr^{-1}
Equatorial Atlantic [b]	10×10^6 mol Se yr^{-1}
Amerasian Basin (per km^2) [a]	0.30 ± 0.16 mol km^{-2} yr^{-1}
World Average [c]	0.32 – 0.47 mol km^{-2} yr^{-1}

[a]This Work; [b]Cutter and Cutter, 2001; [c]Mosher and Duce, 1987.

The atmospheric Arctic Se deposition rate on par with the world average was surprising. The Arctic is typically thought of as a low aerosol region with high seasonality in both precipitation and aerosol concentration where winter months contain 10-40 times more aerosols and have 5 times less monthly precipitation (Barrie, 1986, 1990). The higher precipitation during the summer could prevent aerosol concentrations in the basin from reaching winter maximums by removing windblown aerosols from the Arctic atmosphere.

With the aerosol Se deposition rate established, the source of gaseous Se that explains the high crustal enrichment factor of the aerosols (Fig. 24) can be identified. Anthropogenic emission of Se via fossil fuel combustion are heavily enriched in Se compared to crustal ratios (Ross, 1985). Biogenic release of selenium from the surface ocean also increases the crustal enrichment factor of aerosol Se and has been shown to be closely linked to the biogenic release of dimethyl sulfide (DMS; Amouroux et al., 2001). Arctic phytoplankton have been reported to release 2.0 µmol S m^{-2} d^{-1} (Leck and Persson, 1965; Table 18). The emissions of North Atlantic phytoplankton have an average Se/S molar ratio of 1.4×10^{-4} (Amouroux et al., 2001).

Assuming Arctic phytoplankton emit the same Se/S ratio, Amerasian Basin phytoplankton release 8.6 x 10^5 mol Se yr^{-1} to the atmosphere (Table 11). This release of volatile Se accounts for 43% of the calculated atmospheric deposition flux (2.6 ± 1.3 x 10^6 mol yr^{-1}; Table 11), indicating that 43% of the aerosol Se samples were locally biogenic emission of DMSe and 57% of the aerosol Se came from far away fossil fuel combustion. Melting ice and global warming are expected to increase Arctic DMS production up to 80% by 2080 (Gabric et al., 2005), possibly causing a shift in dominance of EF source from fossil fuel combustion to local biogenic production.

Table 18. Calculations of biogenic release of Se to the atmosphere.

Arctic Volatile Sulfur Emission	Se:S (mol:mol)	Area of the Amerasian Basin	Arctic volatile Se Emission
2.0 µmol S m^{-2} d^{-1}	1.4 x 10^{-4}	8.43 x 10^6 km^2	8.6 x 10^5 mol Se yr^{-1}

CHAPTER 5

CONCLUSIONS

Biogeochemical Cycle

Unlike the Atlantic, Indian, and Pacific Oceans, there was a weaker relationship between selenium species and silicate and phosphate in the Amerasian Basin, suggesting unique internal processes in the Amerasian Basin. Application of empirical relationships between selenium species and silicate and phosphate resulted in the underestimate of selenite and over estimate of selenate concentrations. A slower oxidation rate from selenite to selenate in the Amerasian Basin than in the Pacific, Atlantic, or Indian Oceans is one possibility that would lead to an underestimation of selenite and overestimation of selenate. Identifying transformation rates of selenium species would verify this theory, but physical mixing was too complicated to allow simple advection/diffusion modeling to derive transformation rates (e.g., Measures et al., 1980) or the use of isopycnal mixing and CFC ages to estimate the same parameters (e.g., Cutter and Cutter, 1998).

The various Se data collected and analyzed during this study, combined with physical oceanographic analysis, generated the first comprehensive description of the biogeochemical cycling of Se in the Amerasian Basin (Figure 26). Like the Atlantic and Pacific Oceans, Se enters the Amerasian Basin via atmospheric deposition, riverine transport, and flow from neighboring oceans. Unique to the Amerasian Basin cycle is the apparent slower than normal internal transformation of Se species to the thermodynamically stable form of selenate. When generating the biogeochemical cycling model, each input and removal flux was calculated

independently and errors were given for each flux whenever possible. Total Se input to the Amerasian Basin was calculated adding Pacific and Atlantic inflow fluxes, atmospheric deposition, and riverine flux, resulting in a total input of $1.0 \pm 0.5 \times 10^{8}$ mol yr^{-1} (Table 11). The total removal of Se was calculated by adding Canadian Archipelago, Fram Strait, and shelf and basin sedimentation fluxes, resulting in $1.0 \pm 0.1 \times 10^{8}$ mol yr^{-1} being removed from the water column in the Amerasian Basin (Table 11). The similar ranges for input and removal fluxes suggests that the Se cycle in the Amerasian Basin is in steady state. Interactions between the Atlantic Ocean and the Amerasian Basin were the most dominant relationship in the Se mass balance accounting for 65% of the Se input and 92% of the Se removal processes. The dominance of the Atlantic Ocean is totally based on the water budget for the Arctic and estimated outflow and inflow Se concentrations. Direct measurements of Se in the Fram and Nares Strait, as well as at the Lomonosov Ridge where Eurasian Basin waters enter the Amerasian Basin, would greatly verify the importance of the Atlantic Ocean in the cycling of Se in the Amerasian Basin.

Residence times

To quantitatively assess the Se cycle in the Amerasian Basin, the residence times of Se in the Amerasian Basin were estimated. The residence times of Se relative to the residence times of the water itself affects the manifestation of its biogeochemical cycling. As examples, a long Se residence time compared to a short water residence time makes Se appear to be more conservative, little variations with depth or location, whereas a relatively short Se residence

time allows the processes affecting Se to be fully manifested, there are more variations with depth and location in the basin.

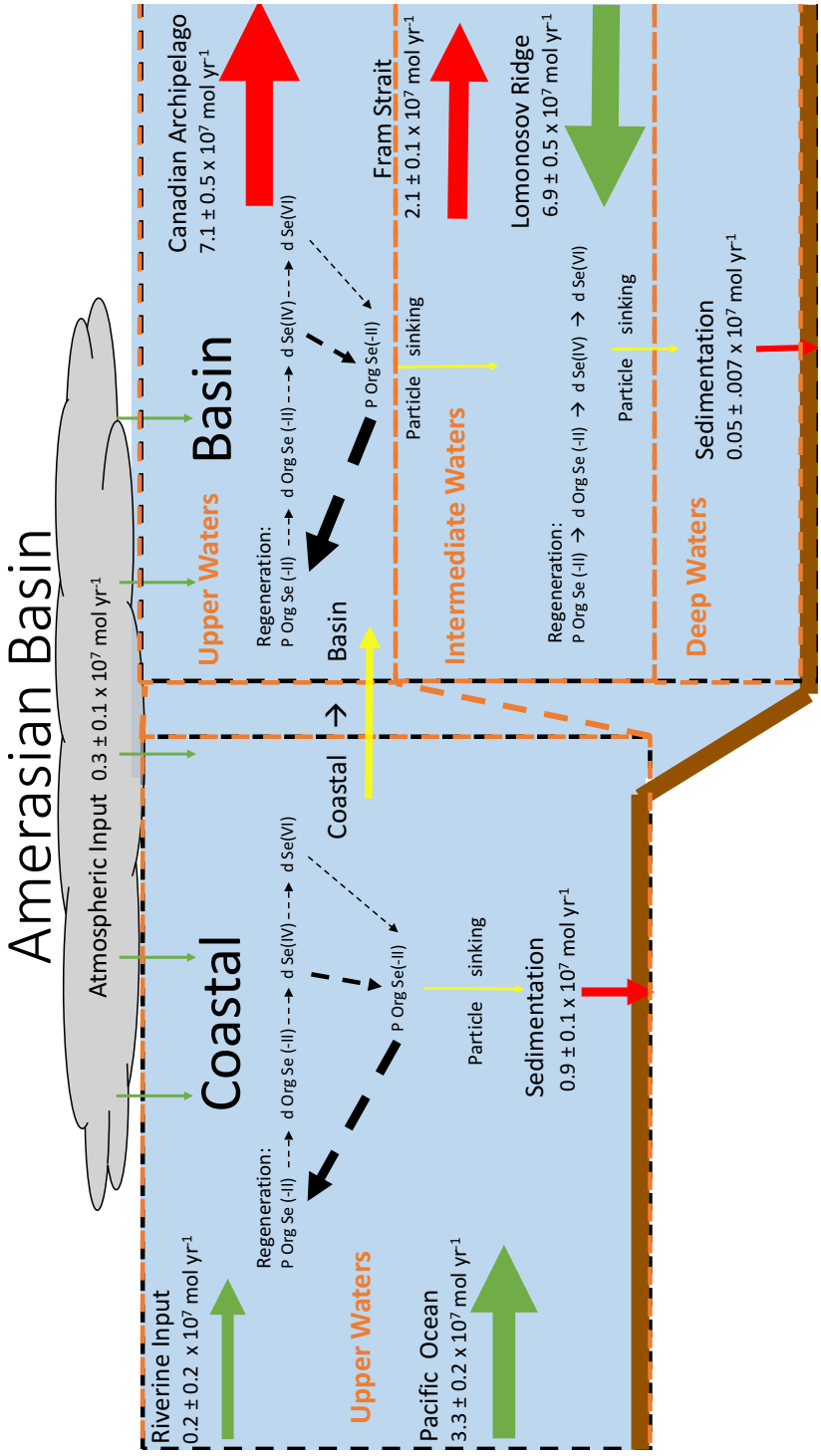

Fig. 26. Biogeochemical cycling of selenium in the Amerasian Basin. Uncertainties are represented as standard deviations from the mean.

Total basin Se residence times (i.e. inventory/input or removal fluxes) were calculated two independent ways by dividing the Amerasian Basin Se inventory (1.6×10^{10} mol Se; Table 19) first by the total Input flux ($1.0 \pm 0.5 \times 10^{8}$ mol Se yr^{-1}) and then by the total removal flux ($1.0 \pm 0.1 \times 10^{8}$ mol Se yr^{-1}; Table 19) giving residence times of 149 ± 112 years and 151± 27 years, respectively (Table 19). Input and removal fluxes that generate the same residence time indicate that the selenium cycle in the Amerasian Basin was at steady state. A residence time of roughly 150 years is about the same as the average water residence time (~113 years; Aagaard and Carmack, 1989) providing an explanation for the similarities and small differences in the vertical profiles and concentrations found in the Amerasian Basin. The overall Se residence time in the Amerasian Basin is the result of a combination of biological processes in three distinct regimes in the basin (e.g. net uptake in surface waters and regeneration at depth).

Table 19. Total basin residence time calculations using input and removal fluxes. Error is reported as standard deviations.

Amerasian Basin Se Inventory (mol Se)	Total Input Flux (mol yr^{-1})	Total Removal Flux (mol $yr^{-1)}$	Basin Residence Time - input (years)	Basin Residence Time - removal (years)
1.6×10^{10}	$1.0 \pm 0.5 \times 10^{8}$	$1.0 \pm 0.1 \times 10^{8}$	149 ± 112	151 ± 27

The Amerasian Basin has three distinct regimes, the shelf, the deep basin water below the Lomonosov Ridge sill, and intermediate basin layer (IBL), the basin water above the Lomonosov Ridge. Both the shelf and the deep basin Se residence times were calculated by dividing their Se inventory by the sedimentation rate. Se transport out of the shelf region and

into the basin was determined to be insignificant and could therefore be ignored because there was no linear relationship between ^{228}Ra activity and total dissolved Se concentrations (Fig. 25). The shelf Se inventory (4.6 ± 0.6 x 10^7 mol; Table 20) divided by the shelf sedimentation rate (1.2 ± 0.5 x 10^7 mol Se yr^{-1}; Table 20) resulted in a residence time of 3.8 ± 0.5 years (Table 20). A short residence time on the shelf is consistent with the high primary productivity and sedimentation rates found on the shelf (Hill and Cota, 2005; Darby et al., 2009).

As described in Chapter 2, deep basin water is found below the Lomonosov Ridge sill depth of 2000 m, minimizing exchange with the other water masses in the Amerasian Basin and results in a ^{14}C age of about 1000 years (MacDonald and Carmack, 1991) and a mean ventilation time of 700 years (Ostlund et al., 1987). The deep basin Se inventory (1.17 ± 0.4 x 10^{10} mol Se; Table 20) divided by the basin sedimentation rate (4.5 ± 0.7 x 10^5 mol yr^{-1}; Table 20) resulted in a Se residence time of 26150 ± 5318 years (Table 20), roughly 30 times that of the ventilation time of the water. A Se residence time that long suggests that Se is essentially conservative in deep water and should be the same concentration throughout the deep basin. However, Se concentrations varied throughout the basin (Figs. 19 – 22) indicating that there must be some deep basin sink of Se not observed in this study, possibly a vertical loss of Se to the overlying water column.

Table 20. Selenium residence time calculations for the shelf and deep water of the Amerasian Basin. Error is reported as standard deviations.

Location	Inventory (mol Se)	Sedimentation Rate (mol yr^{-1})	Residence Time (years)
Shelf	4.6 ± 0.6 x 10^7	1.2 ± 0.5 x 10^7	3.8 ± 0.5 years
Deep Basin Water	1.17 ± 0.4 x 10^{10}	4.5 ± 0.7 x 10^5	26150 ± 5318 years

The intermediate basin layer (IBL) is water above the Lomonosov Ridge, roughly shallower than 2000 m in the Amerasian Basin, and is part of the Arctic Ocean circulation making it different than the relatively isolated deep basin water (Rudels, 2012). A residence time of Se in the IBL was calculated by multiplying the DIA Se in the Amerasian Basin that excluded the deep water layer (843.4 nmol m^{-3}; Table 21) by the volume of the Amerasian basin excluding the deep water (6.75 x 10^{15} m^3; Table 21) then dividing the value by the removal rate via water outflow through the Fram Strait and Canadian Archipelago (9.2 ± 1.1 x 10^7 mol yr^{-1}; Table 11). This calculation gives a residence time of 71 ± 22 years (Table 21). This residence time was longer than the longest ventilation time in these intermediate water depths (40 years; Smethie et al., 2000) indicating that Se is partially recycled in the water column. Although the Se residence time is longer than the water residence time in the IBL, 70 years is still short enough to prevent the slower processes, like the oxidation of selenite to selenate (Cutter and Bruland, 1984), from manifesting itself. Using the typical oxidation rate constant (0.0009 yr^{-1}; Cuter and Bruland, 1984), the normal residence time of selenite can be calculated as 1/oxidation rate constant, resulting in a residence time of ~1000 years. Nowhere in the Amerasian Basin is the water old enough to allow for the full oxidation of dissolved Se, quantitatively confirming the speculation from Chapter 3 that the oxidation of selenite is slower or remains incomplete throughout the Amerasian Basin.

Table 21. Selenium residence time in circulating water masses. Error is reported as standard deviations.

Amerasian Basin DIA	Amerasian Basin volume without deep water	Removal rate via outflow	Residence time
843.4 nmol m^{-3}	6.75 x 10^{15} m^3	9.2 ± 1.1 x 10^7 mol yr^{-1}	71 ± 22 years

Future Work

The Se dataset for the Amerasian Basin is currently lacking important direct measurements that necessitated a lot of assumptions in this thesis. Direct measurements of Se concentrations in the riverine and Atlantic input flows as well as Canadian Archipelago and Fram Strait removal flows would greatly increase the accuracy of the Amerasian Se budget. Determining the Se concentration of deep basin sediment would remove the necessity of assuming coastal sediment had the same Se concentration as basin sediment when calculating the deep basin sedimentation rate.

Unfortunately, this work did not look at the impact sea ice has on the Se cycle in the Amerasian Basin. No ice cores were analyzed for Se and only one near surface, under ice profile was conducted. Sea ice is a unique attribute of the polar oceans and is a major missing piece in the selenium budget for the Amerasian Basin that should be addressed in future expeditions.

The Arctic will continue to change in response to a warming climate. Ice free summers, estimated to occur within 30 years (Wang and Overland, 2012), might cause selenium to behave more like it does in the Pacific and Atlantic with pronounced depletion and regeneration zones (Measures et al., 1980, Cutter and Bruland, 1984, Cutter and Cutter, 1995, 2001). However, increased river discharge (Peterson et al., 2002) and warming could increase stratification (Woodgate et al., 2012) and potentially limit nutrient supply to photosynthetic organisms at the surface, causing the Amerasian Basin to behave more like an oligotrophic ocean. Continued monitoring of the Arctic will allow for these changes to be observed and predictions improved. Thus, future work should return to the sampling locations of the Arctic

U.S. GEOTRACES GN03 transect, collect the same types of samples, and expand the data set by performing selenium analyses on ice samples. The findings presented in this study provide the baseline that will allow for the identification of any future changes to the biogeochemical cycling of Se in the Amerasian Basin.

REFERENCES

Aagaard K. (1981) On the deep circulation in the Arctic Ocean. *Deep Sea Res. A Oceanogr. Res. Pap.* **28**, 251-268.

Aagaard K, Coachman L. K., and Carmack E. (1981) On the halocline of the Arctic Ocean. *Deep Sea Res. A Oceanogr. Res. Pap.* **28**, 529-545.

Aagaard K., and Carmack E. C. (1989) The role of sea ice and other fresh water in the Arctic circulation. *J. geophys. Res*. **94**, 14485-14489.

Aagaard K., Swift J. H., and Carmack E. C. (1985) Thermohaline circulation in the Arctic Mediterranean seas. *J. Geophys. Res.* **90**, 4833-4846.

Amouroux D., Liss P. S., Tessier E., Hamren-Larsson M., and Donard O. F. (2001) Role of oceans as biogenic sources of selenium. *Earth Planet. Sci. Lett.* **189**, 277-283.

Andrews J. T., and Dunhill G. (2004) Early to mid-Holocene Atlantic water influx and deglacial meltwater events, Beaufort Sea slope, Arctic Ocean. *Quaternary Res.* **61**, 14-21.

Apte S. C., Howard A. G., Morris R..J., and McCartney M. J. (1986) Arsenic, antimony and selenium speciation during a spring phytoplankton bloom in a closed experimental ecosystem. *Mar. Chem.* **20**, 119-130.

Arimoto R., Duce R., Savoie D., and Prospero J. (1992) Trace elements in aerosol particles from Bermuda and Barbados: Concentrations, sources and relationships to aerosol sulfate. *J. Atm. Chem.* **14**, 439-457.

Barrie L. A. (1986) Arctic air pollution: an overview of current knowledge. *Atm. Environ.* **20**, 643-663.

Barrie L. A. (1990) Arctic air pollution: A case study of continent-to-ocean-to-continent transport. *The Long-Range Atmospheric Transport of Natural and Contaminant Substances.* Springer, Berlin, Germany. pp 137-148.

Berner R. A. (1980) *Early diagenesis*. A theoretical approach: Princeton University Press, Princeton.

Bird K. J., Charpentier R. R., Gautier D. L., Houseknecht D. W., Klett T. R., Pitman J. K., Moore T. E., Schenk C. J., Tennyson M. E., and Wandrey C. R. (2008) Estimates of undiscovered oil and gas north of the Arctic Circle. In *Circum-Arctic resource appraisal*. Geological Survey (US). Report 2327-6932.

Bishop J. K., Lam P. J., and Wood T.J. (2012) Getting good particles: Accurate sampling of particles by large volume in-situ filtration. *Limnol. Oceanogr. Methods* **10**, 681-710.

Black E. E. (2018)*An investigation of basin-scale controls on upper ocean export and remineralization*. Diss. Massachuestes Institute of Technology and Woods Hole Oceanography Institution.

Bourgoin B., and Risk M. (1987) Vanadium contamination monitored by an Arctic bivalve, Cyrtodaria kurriana. *Bulletin of Environ. Contamination Toxicol.* **39**, 1063-1068.

Carmack E. C., Yamamoto-Kawai M., Haine T. W., Bacon S., Bluhm B. A., Lique C., Melling H., Polyakov I.V., Straneo F., and Timmermans M. L. (2016) Freshwater and its role in the Arctic Marine System: Sources, disposition, storage, export, and physical and biogeochemical consequences in the Arctic and global oceans. *J. Geophys. Res. Biogeosci.***121**, 675-717.

Charette M. A., Lam P. J., Lohan M. C., Kwon E. Y., Hatje V., Jeandel C., Shiller A. M., Cutter G. A., Thomas A., and Boyd P. W. (2016) Coastal ocean and shelf-sea biogeochemical cycling of trace elements and isotopes: lessons learned from GEOTRACES. *Phil. Trans. Res. Soc. A* **374**,.

Clark L. C., Combs G. F., Turnbull B. W., Slate E. H., Chalker D. K., Chow J., Davis L. S., Glover R. A., Graham G. F., and Gross E. G. (1996) Effects of selenium supplementation for cancer prevention in patients with carcinoma of the skin: a randomized controlled trial. *Jama* **276**, 1957-1963.

Codispoti L., Kelly V., Thessen A., Matrai P., Suttles S., Hill V., Steele M., and Light B. (2013) Synthesis of primary production in the Arctic Ocean: III. Nitrate and phosphate based estimates of net community production. *Prog. Oceanogr.* **110**, 126-150.

Cotton F. A., and Wilkinson G. (1988) *Advanced Inorganic Chemistry*. Wiley, New York.

Cutter G. A. (1978) Species determination of selenium in natural waters. *Analytica Chimica Acta* **98**, 59-66.

Cutter G. A. (1982) Selenium in reducing waters. *Science* **217**, 829-831.

Cutter G. A. (1983) Elimination of nitrite interference in the determination of selenium by hydride generation. *Analytica Chimica Acta* **149**, 391-394.

Cutter G. A. (1985) Determination of selenium speciation in biogenic particles and sediments. *Analytical Chem.* **57**, 2951-2955.

Cutter G. A. (1989a) The estuarine behaviour of selenium in San Francisco Bay. *Estuarine, Coastal and Shelf Sci.* **28**, 13-34.

Cutter G. A. (1989b) *Occurrence and Distribution of Selenium inFreshwater systems*. CRC Press, Boca Raton, Florida.

Cutter G. A. (1993) Metalloids in wet deposition on Bermuda: concentrations, sources, and fluxes. *J. Geophys Res Atm.* **98**, 16777-16786.

Cutter G. A., and Bruland K. W. (1984) The marine biogeochemistry of selenium: a re-evaluation. *Limnol. and Oceanogr.* **29**, 1179-1192.

Cutter G. A., and Bruland K. W. (2012) Rapid and noncontaminating sampling system for trace elements in global ocean surveys. *Limnol. Oceanogr. Methods* **10**, 425-436.

Cutter G. A., and Cutter L. S.. (1995) Behavior of dissolved antimony, arsenic, and selenium in the Atlantic Ocean. *Mar. Chem.* **49**, 295-306.

Cutter G. A., and Cutter L. S. (1998) Metalloids in the high latitude North Atlantic Ocean: sources and internal cycling. *Mar. Chem.* **61**, 25-36.

Cutter G. A., and Cutter L. S. (2001) Sources and cycling of selenium in the western and equatorial Atlantic Ocean. *Deep Sea Res. II Top. Stud. Oceanogr.* **48**, 2917-2931.

Cutter G. A. , and Cutter L. S. (2004) Selenium biogeochemistry in the San Francisco Bay estuary: changes in water column behavior. *Estuarine, Coastal and Shelf Sci.* **61**, 463-476.

Darby D. A., Ortiz J., Polyak L., Lund S., Jakobsson M., and Woodgate R. A. (2009) The role of currents and sea ice in both slowly deposited central Arctic and rapidly deposited Chukchi–Alaskan margin sediments. *Global and Planet. Change* **68**, 58-72.

Doblin M. A., Baines S. B., Cutter L. S., and Cutter G. A. (2006) Sources and biogeochemical cycling of particulate selenium in the San Francisco Bay estuary. *Estuarine, Coastal and Shelf Sci.* **67**, 681-694.

Fernández-Méndez M., Katlein C., Rabe B., Nicolaus M., Peeken I., Bakker K., Flores H., and Boetius A. (2015) Photosynthetic production in the central Arctic Ocean during the record sea-ice minimum in 2012. *Biogeosci.* **12**, 3525-3549.

Fisher J. A., Jacob D. J., Soerensen A. L., Amos H. M., Steffen A., and Sunderland E.M. (2012) Riverine source of Arctic Ocean mercury inferred from atmospheric observations. *Nature Geosci.* **5**, 499-504.

Ganther H. E. (1999) Selenium metabolism, selenoproteins and mechanisms of cancer prevention: complexities with thioredoxin reductase. *Carcinogenesis* **20**, 1657-1666.

Goudie A. S. (2013) The human impact on the natural environment: past, present, and future: John Wiley & Sons, Hoboken.

Grantz A., Phillips R., Mullen M., Starratt S., Jones G. A., Naidu A. S., and Finney B. (1996) Character, paleoenvironment, rate of accumulation, and evidence for seismic triggering of Holocene turbidites, Canada Abyssal Plain, Arctic Ocean. *Mar. Geol.* **133**, 51-73.

Hamilton J. M. (2011) *The challenges of deep water Arctic development.* International Society of Offshore and Polar Engineers. pp.1.

Hill V., and Cota G. (2005) Spatial patterns of primary production on the shelf, slope and basin of the Western Arctic in 2002. *Deep Sea Res II Top. Stud. Oceanogr.* **52**, 3344-3354.

Hill V. J., Matrai P. A., Olson E., Suttles S., Steele M., Codispoti L., and Zimmerman R. C. (2013) Synthesis of integrated primary production in the Arctic Ocean: II. In situ and remotely sensed estimates. *Prog. Oceanogr.* **110**, 107-125.

Holmes R. M., Shiklomanov A. I., Tank S. E., McClelland J. W., and Tretiakov M. (2015) Arctic Report Card: Update for 2015. *National Oceanic and Atmosphere Administrations*.

Jakobsson M., Macnab R., Mayer L., Anderson R., Edwards M., Hatzky J., Schenke H. W., and Johnson P. (2008) An improved bathymetric portrayal of the Arctic Ocean: Implications for ocean modeling and geological, geophysical and oceanographic analyses. *Geophys. Res. Lett.* **35**, L7.

Jones E. P., Anderson L. G., and Swift J.H. (1998) Distribution of Atlantic and Pacific waters in the upper Arctic Ocean: Implications for circulation. Geophysical Research Letters **25**, 765-768.

Jones E. P., Rudels B., and Anderson L. G. (1995) Deep waters of the Arctic Ocean: origins and circulation. Deep Sea Research Part I: Oceanographic Research Papers 42(5):737-760.

Kadko D., and Muench R. (2005) Evaluation of shelf–basin interaction in the western Arctic by use of short-lived radium isotopes: The importance of mesoscale processes. Deep Sea Research Part II: Top. Stud. Oceanogr. **52**, 3227-3244.

Kavlak G., and Graedel T. (2013) Global anthropogenic selenium cycles for 1940-2010. *Res. Conserv. Recycl.* **73**, 17-22.

Leck C, Persson C. (1996) The central Arctic Ocean as a source of dimethyl sulfide Seasonal variability in relation to biological activity. *Tellus B: Chem. Phys. Meteorol.* **48**, 156-177.

Lippard S. J., and Berg J. M. (1994) *Principles of bioinorganic chemistry*. University Science Books, Mill Valley. pp. 115

Lovvorn J. R., Raisbeck M. F., Cooper L. W., Cutter G. A., Miller M. W., Brooks M. L., Grebmeier J. M., Matz A. C., and Schaefer C. M. (2013) Wintering eiders acquire exceptional Se and Cd burdens in the Bering Sea: physiological and oceanographic factors. *Mar. Ecol. Prog. Series* **489**, 245-261.

Macdonald R., and Carmack E. (1991) Age of Canada Basin deep waters: A way to estimate primary production for the Arctic Ocean. *Science(Washington)* **254**, 1348-1350.

Maenhaut W., Cornille P., Pacyna J. M., and Vitols V. (1989) Trace element composition and origin of the atmospheric aerosol in the Norwegian Arctic. *Atm. Environ.* **23**, 2551-2569.

Marnela M., Rudels B., Goszczko I., Beszczynska-Möller A., and Schauer U. (2016. Fram Strait and Greenland Sea transports, water masses, and water mass transformations 1999–2010 (and beyond). *J. of Geophys. Res. Oceans* **121**, 2314-2346.

McClelland J. W., Holmes R. M., Peterson B. J., Amon R., Brabets T., Cooper L., Gibson J., Gordeev V. V., Guay C., and Milburn D. (2008) Development of a pan-Arctic database for river chemistry. *Eos Transactions American Geophys. Union* **89**, 217-218.

McLaughlin F. A., Carmack E. C., Macdonald R. W., Melling H., Swift J. H., Wheeler P. A., Sherr B. F., and Sherr E. B. (2004) The joint roles of Pacific and Atlantic-origin waters in the Canada Basin, 1997–1998. *Deep Sea Res. I Oceanogr. Res. Pap.* **51**, 107-128.

McNeal J. M., snd Balistrieri L. S. (1989) Geochemistry and occurrence of selenium: an overview. In *Selenium in Agriculture and the Environment*(ed. L. W. Jacobs). SSSA Special Publications, Madison, pp. 1-13.

Measures C., and Burton J. (1978) Behaviour and speciation of dissolved selenium in estuarine waters. *Nature* **273**, 293-295.

Measures C., and Burton J. (1980) The vertical distribution and oxidation states of dissolved selenium in the northeast Atlantic Ocean and their relationship to biological processes. *Earth Planet Sci. Lett.* **46**, 385-396.

Measures C., Grant B., Mangum B., and Edmond J. (1983) *The relationship of the distribution of dissolved selenium IV and VI in three oceans to physical and biological processes. Trace metals in sea water*. Springer Berlin, Germany. pp 73-83.

Measures C., McDuff R., and Edmond J. (1980) Selenium redox chemistry at GEOSECS I re-occupation. *Earth and Planet. Sci. Lett.* **49**, 102-108.

Meseck S. L, and Cutter G. A. (2006) Evaluating the biogeochemical cycle of selenium in San Francisco Bay through modeling. *Limnol. Oceanog.* **51**, 2018-2032.

Meyer J., Moulis J-M., Gaillard J., and Lutz M. (1992) Replacement Of Sulfur By Selenium In Iron—Sulfur Proteins. *Advances in inorganic chem.* **38**, 73-115.

Morison J., Steele M., and Andersen R. (1998) Hydrography of the upper Arctic Ocean measured from the nuclear submarine USS Pargo. *Deep Sea Res. I Oceanogr. Res. Pap.* **45**, 15-38.

Morton P. L., Landing W. M., Hsu S. C., Milne A., Aguilar-Islas A. M., Baker A. R., Bowie A. R., Buck C. S., Gao Y., and Gichuki S. (2013) Methods for the sampling and analysis of marine aerosols: results from the 2008 GEOTRACES aerosol intercalibration experiment. *Limnol. Oceanogr Meth.* **11**, 62-78.

Mosher B. W., and Duce R. A. (1987). A Global Atmospheric Selenium Budget. *J. Geophys. Res. Atm.* **92**, 13,289-213,298.

Mosher B. W., Duce R. A., Prospero J. M., and Savoie D. L. (1987) Atmospheric selenium: geographical distribution and ocean to atmosphere flux in the Pacific. *J. Geophys. Res. Atm.* **92**, 13277-13287.

Moxon A. L., Olson O. E., and Searight W. V. (1939) *Selenium in Rocks, Soils, and Plants*. South Dakota State College of Agriculture and Machanic Arts, Brookings, SD.

Münchow A., and Melling H. (2015) Volume and freshwater flux to the West of Greenland: Nares Strait 2003-09. *J. Phys. Oceanogr.* **10**, 1-8.

Nuttall K. L., and Allen F. S. (1984) Selenium detoxification of heavy metals: a possible mechanism for the blood plasma. *Inorganica Chimica Acta* **92**, 187-189.

Ostlund H. G., Possnert G., and Swift J. H. (1987) ventilation rate of the deep Arctic Ocean from carbon 14 data. *J Geophys. Res. Oceans* **92**, 3769-3777.

Pachauri R. K., Allen M. R., Barros V. R., Broome J., Cramer W., Christ R., Church J. A., Clarke L., Dahe Q., and Dasgupta P. (2014) Climate change 2014: synthesis report. Contribution of Working Groups I, II and III to the fifth assessment report of the Intergovernmental Panel on Climate Change. IPCC.

Pacyna J. M., and Pacyna E. G. (2001) An assessment of global and regional emissions of trace metals to the atmosphere from anthropogenic sources worldwide. *Environ. Rev.* **9**, 269-298.

Peterson B. J., Holmes R. M., McClelland J. W., Vörösmarty C. J., Lammers R. B., Shiklomanov A. I., Shiklomanov I. A., and Rahmstorf S. (2002) Increasing river discharge to the Arctic Ocean. *Science* **298**, 2171-2173.

Ranville M. A., Cutter G. A., Buck C. S., Landing W. M., Cutter L. S., Resing J. A., and Flegal A. R. (2010) Aeolian contamination of Se and Ag in the North Pacific from Asian fossil fuel combustion. *Environ sci technol.* **44**, 1587-1593.

Reeves R. R., Ewins P. J., Agbayani S., Heide-Jørgensen M. P., Kovacs K. M., Lydersen C., Suydam R., Elliott W., Polet G., and van Dijk Y. (2014) Distribution of endemic cetaceans in relation to hydrocarbon development and commercial shipping in a warming Arctic. *Mar. Policy* **44**, 375-389.

Riedel G. F., Sanders J. G., and Gilmour C. C. (1996) Uptake, transformation, and impact of selenium in freshwater phytoplankton and bacterioplankton communities. Aquatic *Microb. Ecol.* **11**, 43-51.

Roeske T., vd Loeff M. R., Middag R., and Bakker K. (2012) Deep water circulation and composition in the Arctic Ocean by dissolved barium, aluminium and silicate. *Mar. Chem.* **132**, 56-67.

Rosen B. P., and Liu Z. (2009) Transport pathways for arsenic and selenium: a minireview. *Environ. international* **35**, 512-515.

Ross HB. 1985. An atmospheric selenium budget for the region 30 N to 90 N. *Tellus B* **37**, 78-90.

Rudels B. (2009) Arctic Ocean Circulation. In: Steele JH, Turekian KK, Thorpe SA, editors. *Encyclopedia of Ocean Sciences*. 2nd ed. Amsterdam, Netherlands: Elsevier Ltd. p 211-225.

Rudels B. (2012) Arctic Ocean circulation and variability-advection and external forcing encounter constraints and local processes. *Ocean Science*. **8**, 261-286.

Rudels B., Jones E., Anderson L., and Kattner G. (1994) On the intermediate depth waters of the Arctic Ocean. In *The polar oceans and their role in shaping the global environment* pp. 33-46.

Rudels B., Jones E. P., Schauer U., and Eriksson P. (2004) Atlantic sources of the Arctic Ocean surface and halocline waters. *Polar Res.* **23**, 181-208.

Rue EL, Smith GJ, Cutter GA, Bruland KW. (1997) The response of trace element redox couples to suboxic conditions in the water column. *Deep Sea Res. I Oceanogr. Res. Pap.* **44**, 113-134.

Ryan-Harshman M., and Aldoori W. (2005) The relevance of selenium to immunity, cancer, and infectious/inflammatory diseases. *Canadian J. Dietetic Prac. Res.* **66**, 98-102.

Sakshaug E. (2004) Primary and secondary production in the Arctic Seas. In *The organic carbon cycle in the Arctic Ocean*. Springer, Berlin, Germany. pp 57-81.

Schauer U, Fahrbach E, Osterhus S, Rohardt G. 2004. Arctic warming through the Fram Strait: Oceanic heat transport from 3 years of measurements. *J Geophys. Rese. Oceans* **109**,.

Shamberger R. (1983) The Biogeochemistry of Selenium. New York, NY: Plenum.

Sherrard J. C., Hunter K. A., and Boyd P. W. (2004) Selenium speciation in subantarctic and subtropical waters east of New Zealand: trends and temporal variations. *Deep Sea Res. I Oceanogr. Res. Pap.* **51**, 491-506.

Smedsrud L. H., Esau I., Ingvaldsen R. B., Eldevik T., Haugan P. M., Li C., Lien V. S., Olsen A., Omar A. M., and Otterå O. H. (2013) The role of the Barents Sea in the Arctic climate system. *Review Geophys.* **51**, 415-449.

Smethie W. M., Schlosser P., Bönisch G., and Hopkins T. S. (2000) Renewal and circulation of intermediate waters in the Canadian Basin observed on the SCICEX 96 cruise. *J. Geophys. Res. Oceans* **105**, 1105-1121.

Spallholz J. E. (1994) On the nature of selenium toxicity and carcinostatic activity. *Free Radical Biol. and Med.* **17**, 45-64.

Steinbrenner H., and Sies H. (2009) Protection against reactive oxygen species by selenoproteins. *Biochimica et Biophysica Acta Gen. Sub.* **1790**, 1478-1485.

Sun H-J., Rathinasabapathi B., Wu B., Luo J., Pu L-P., and Ma L. Q. (2014) Arsenic and selenium toxicity and their interactive effects in humans. *Environ. International* **69**, 148-158.

Swift J. H, Jones E. P., Aagaard K., Carmack E. C., Hingston .M, Macdonald R. W., McLaughlin F. A., and Perkin R. G. (1997) Waters of the Makarov and Canada basins. *Deep Sea Res. II Top. Stud. Oceanogr.* **44**, 1503-1529.

Takayanagi K., and Wong G. T. (1984) Total selenium and selenium (IV) in the James River estuary and southern Chesapeake Bay. Estuarine, Coastal and Shelf Science **18**, 113-119.

Taylor J. (1997) *Introduction to error analysis, the study of uncertainties in physical measurements.* Univerisity Science Books, New York, NY.

Taylor S. R., and McLennan S. M. (1985) *The continental crust: its composition and evolution. United States*. Blackwell Scientific Pub, Palo Alto, CA.

Terzaghi K., Peck R. B., and Mesri G. (1996) *Soil mechanics in engineering practice*. John Wiley & Sons Publication, Hoboken.

Uematsu M., Duce R. A., and Prospero J. M. (1985) Deposition of atmospheric mineral particles in the North Pacific Ocean. Journal of Atmospheric Chemistry **3**, 123-138.

Wang M., Overland J. E. (2012) A sea ice free summer Arctic within 30 years: An update from CMIP5 models. Geophysical Research Letters **39**, L18501.

Wang Q., Kim D., Dionysiou D. D., Sorial G. A., and Timberlake D. (2004) Sources and remediation for mercury contamination in aquatic systems—a literature review. Environmental pollution **131**, 323-336.

Woodgate R. A. (2017) Increases in the Pacific inflow to the Arctic from 1990 to 2015, and insights into seasonal trends and driving mechanisms from year-round Bering Strait mooring data. *Prog. in Ocean.* **160**, 124-154.

Woodgate R. A, Aagaard K., Muench R. D., Gunn J., Björk G., Rudels B., Roach A., and Schauer U. (2001) The Arctic Ocean boundary current along the Eurasian slope and the adjacent Lomonosov Ridge: Water mass properties, transports and transformations from moored instruments. *Deep Sea Res. I Oceanogr. Res. Pap*. **48**, 1757-1792.

Wrench J., and Measures C. I. (1982) Temporal variations in dissolved selenium in a coastal ecosystem. *Nature* **299**,431-433.

Yoneda S., and Suzuki K. T. (1997) Detoxification of mercury by selenium by binding of equimolar Hg–Se complex to a specific plasma protein. *Tox. and applied pharm.* **143**, 274-280.

VITA

Kyle A. McQuiggan

Department of Ocean, Earth, and Atmospheric Sciences

4600 Elkhorn Avenue

Norfolk VA, 23529

Education

Master of Science in Ocean, Earth, and Atmospheric Science at Old Dominion University, Norfolk, VA, May, 2018 "Biogeochemical cycling of selenium in the Amerasian Basin"

Bachelor of Science in Geology minor in Biology at Union College, Schenectady, NY, May, 2014 "A 5,000-year record of trace elements and stable isotopes in a Belgian speleothem"

Academic Presentations

Association for the Science of Limnology and Oceanography Honolulu, HI February, 2016. Poster: "Biogeochemical cycling of selenium in the Arctic Ocean"

Geological Society of America Denver, CO, November, 2009. Poster: "A 5,000-year record of trace elements and stable isotopes in a Belgian speleothem"